Title: A peptide that regulates metalation and function of the *Arabidopsis* ethylene receptor

Authors:
Anna J. Mudge[1]†, Saher Mehdi[1]†‡, Will Michaels[1,2]†, Beatriz Orosa-Puente[1]‡‡, Weiran Shen[1], Charlie Tomlinson[2]‡‡‡, Wenbin Wei[1], Claudia Hoppen[3], Buket Uzun[3], Dipan Roy[1], Flora M. Hetherington[1]‡‡‡‡, Jennifer F. Topping[1], Ari Sadanandom[1], Georg Groth[3], Nigel J. Robinson[1,2*], Keith Lindsey[1*]

Affiliations:
[1]*Department of Biosciences, Durham University, Durham, UK*
[2]*Department of Chemistry, Durham University, Durham, UK*
[3]*Institute of Biochemical Plant Physiology, Heinrich Heine University Düsseldorf, D-40204 Düsseldorf, Germany*

†These authors contributed equally to this work
‡Present address: wellOwise Research and Development, IIITD Innovation & Incubation Centre, New Delhi, Delhi - 110020, India.
‡‡Present address: School of Biological Sciences, University of Edinburgh, Edinburgh EH9 3FF, UK; and Centro Singular de Investigación en Química Biolóxica e Materiais Moleculares (CIQUS) and Departamento de Química Orgánica, 15782, Universidade de Santiago de Compostela, Spain
‡‡‡Present address: Department of Biology, University of York, Heslington, York YO10 5DD, U.K.
‡‡‡‡Present address: University of Bath, Claverton Down, Bath BA2 7AY, U.K.

*Joint corresponding authors: keith.lindsey@durham.ac.uk; nigel.robinson@durham.ac.uk

Abstract:
Ethylene signalling represents one of the classic hormonal pathways in plants, with diverse roles in development and stress responses. The dimeric ethylene receptor localizes to the endoplasmic reticulum (ER) and contains Cu(I) ions essential for ethylene binding and signalling. As for other vesicular cupro-proteins, the final step of Cu(I) maturation at the ER is undefined. We previously discovered that mutants in the *Arabidopsis* gene *POLARIS* (*PLS*), encoding a 36 amino acid peptide, exhibit enhanced ethylene signalling responses. Here we report a 1:2 thiol-dependent Cu(I):PLS_2 complex, with an affinity of 3.79 (±1.5) x10^{19} M^{-2}. We demonstrate PLS interactions with the transmembrane domain of receptor protein ETR1, the Cu(I) chaperones ATX1 and CCH, and Cu(I)-transporting P_{1B}-type ATPase RAN1. Formation of Cu(I)-dependent PLS-cuproprotein interactions at the ER provides a mechanism to modulate the metalation of ETR1, thereby regulating its activity and representing a novel mechanism for plant hormone receptor regulation.

Significance statement: Ethylene signalling represents one of the classic hormonal pathways in plants, with diverse roles in development and stress responses. The dimeric ethylene receptor localizes to the endoplasmic reticulum (ER) and contains Cu(I) ions essential for ethylene binding and signalling. The *polaris* (*pls*) mutant of *Arabidopsis* has been shown to exhibit defective ethylene responses. Here we show that the *POLARIS* gene product, a 36 amino acids

peptide, binds copper and interacts with the ethylene hormone receptor to regulate its activity in a tissue-specific manner.

Main text

Ethylene is used by plants as a gaseous hormone to regulate many aspects of development and responses to biotic and abiotic stresses (*1*). It is perceived by a family of receptors that, in *Arabidopsis*, comprises 5 members, ETR1 (ETHYLENE RESPONSE 1), ERS1 (ETHYLENE RESPONSE SENSOR 1), ERS2, ETR2, and EIN4 (ETHYLENE-INSENSITIVE 4) (*2-5*) located on the endoplasmic reticulum (ER) (*6, 7*). The receptors are related to bacterial two-component systems (*2*), form dimers through disulphide bonding at the N-terminal hydrophobic domains (*8, 9*) and contain Cu(I) ions bound to residues Cys65 and His69, essential for ethylene binding and signal transduction (*10, 11*). In the absence of ethylene these receptors activate a negative regulator CTR1 (CONSTITUTIVE TRIPLE RESPONSE 1), which is a mitogen-activated protein kinase kinase kinase (MAPKKK), so preventing ethylene responses (*12, 13*). Mechanisms by which receptor activity is regulated are not fully understood. We describe here a molecular function for the PLS peptide, previously implicated in ethylene signalling (*14*), and a proposed model for its role in ethylene receptor function and plant development.

Introduction of copper to the ER and ethylene receptor requires the RAN1 (RESPONSIVE TO ANTAGONIST1) protein. This is a predicted copper-transporting P-type ATPase homologous to the yeast Ccc2p and to human Menkes and Wilson disease proteins (*15*). Strong loss-of-function mutants of *RAN1* in *Arabidopsis* (e.g. *ran1-3*, *ran1-4*) exhibit an enhanced ethylene signalling response (*16*), consistent with a loss of receptor function, and similar to higher order loss-of-function receptor mutants, which also show an ethylene hypersignalling phenotype (*17*). Mechanisms of copper homeostasis at ETR1 are unknown, and indeed this is true for other compartmentalized cuproproteins supplied with copper, for example via Ccc2p, Menkes or Wilson ATPases. RAN1 in Arabidopsis has been found to localize to endomembrane systems, including *trans*-Golgi and ER compartments, and is necessary for both the biogenesis of ethylene receptors and copper homeostasis during plant development (*16*). There is also evidence that RAN1 interacts directly with ETR1 and the copper chaperones ANTIOXIDANT1 (ATX1) and COPPER TRANSPORT PROTEIN (CCH), suggestive of a transfer of copper between proteins to deliver it to the ethylene receptor as part of the receptor biogenesis pathway at the ER (*18*).

Our understanding of the molecular mechanism of copper delivery to the receptor is still incomplete, however. For example, is metalation of the receptor regulated in a tissue-specific way or in response to the hormonal environment in a tissue? Is this process part of the crosstalk mechanism with other hormone signaling pathways? It is well established that ethylene signaling interacts with and is impacted by other hormonal pathways, but does this influence receptor metalation and does this have developmental consequences? In this paper we propose a model in which a new component of the metalation pathway is identified, which provides cell type specificity and a crosstalk regulatory mechanism for ethylene responses, through copper delivery control to the ethylene receptor.

Results

The POLARIS peptide is a negative regulator of ethylene responses

The *POLARIS* gene of *Arabidopsis* (AT4G39403) encodes a 36 amino acids peptide (Fig. 1a) translated from a low-abundance transcript that, in light-grown seedlings, is most abundant in the

embryo and silique, seedling root tip and leaf vascular tissues, also reflected in promoter-reporter expression patterns (Fig. S1; *19*). We have previously shown that the loss-of-function *pls* mutant has some phenotypic similarities to *ran1* loss-of-function alleles and to *ctr1*, exhibiting a triple response phenotype (short hypocotyl and root, exaggerated apical hook, radial expansion) in the dark in the absence of ethylene (*14*), and a short root in light-grown seedlings, consistent with its expression in the root meristem in light-grown seedlings (Fig. 1b). Transgenic complementation of the mutant by the *PLS* gene suppresses the mutant phenotype (*19*). The *pls* mutant phenotype is rescued by the gain-of-function ethylene resistant mutation *etr1-1* and pharmacological inhibition of ethylene signalling by silver ions (*14*). Ethylene gas production in the *pls* mutant is at wildtype levels, indicating the peptide may play a role in ethylene signalling rather than biosynthesis (*14*). *PLS* transgenic overexpressers (PLSOx seedlings) in contrast exhibit a suppression of the triple response phenotype when grown in the presence of the ethylene precursor ACC, similar to the gain of function *etr1-1* mutant, but this suppression is incomplete (PLSOx seedlings show some response to ACC; *14, 19*); and they suppress the *ctr1* mutant phenotype, indicating that the PLS peptide acts upstream of CTR1 (*14*). However, this repression of the PLSOx phenotype by *ctr1* also is incomplete, with some elongation of the hypocotyl and root in the PLSOx/*ctr1* cross compared to the *ctr1* mutant in the light, and a slightly longer root for the PLSOx/*ctr1* cross grown in air in the dark (*14*). These observations are indicative of some complexity in the relationship between CTR1 and PLS.

To further investigate the *pls* molecular phenotype, we carried out an RNA-seq analysis on loss-of-function *pls* mutant and PLSOx transgenic overexpressor seedlings to identify differentially regulated genes, with mutant and overexpressor each compared with wildtype seedlings of the same ecotype as controls. The *pls* mutant expresses no full length PLS coding sequence due to a T-DNA insertion in the coding region of *PLS* and disrupting function (*19*), while the PLSOx seedlings express significantly higher levels of *PLS* transcript compared to wild-type ($\log_2$ fold 10.8, *padj* value = 2.02×10^{-33}; Tables S1, S2). 836 genes were significantly up-regulated and 292 down-regulated in the *pls* mutant compared to wildtype control seedlings (padj value < 0.05) (Table S1). 1487 genes were significantly up-regulated and 1281 down-regulated in PLSOx seedlings compared to wildtype (padj value < 0.05; Table S2). Gene Ontology (GO) analysis of genes upregulated in *pls* mutant seedlings compared to wildtype showed significant enrichment of genes associated with responses to hormone signalling, biotic and abiotic defence responses, and cell death (Table S3; Fig. S2a). Out of 307 GO:0009723 (response to ethylene) genes, 25 were significantly up-regulated and 7 down-regulated in the *pls* mutant compared with the wildtype, with 40 up-regulated and 18 down-regulated in the PLSOx seedlings (Fig. 1c; Table S3, S4, S5 and S6, *20*), indicating a requirement for control over *PLS* expression levels for correct ethylene responses. While GO:0009723 (response to ethylene) is significantly enriched in genes up-regulated in the *pls* mutant compared to wildtype (*FDR = 0.00062*; Table S3), a large number of up-regulated genes in *pls* are significantly associated with immunity, response to pathogens and hypersensitive response (Table S3 and Fig. S2a). Down-regulated genes in *pls* were significantly enriched in GO categories of hormone biosynthetic processes (GO:0042446, *FDR = 0.038*), hormone metabolic process (GO:0042445, *FDR = 0.0096*) and regulation of hormone levels (GO:0010817, *FDR = 0.0013*) (Table S4, Fig. S2b; *20*), consistent with our previous studies that described PLS-dependent crosstalk between ethylene, auxin and cytokinin signalling (*21, 22, 23*). In PLSOx overexpressors, both up- and down-regulated genes similarly included those associated with GO terms hormone response, stress response and immune response, and genes associated with photosynthesis are downregulated in PLSOx seedlings, consistent with repressed photosynthetic activity in root tips

142 (Table S5 and S6, Fig. S2c, d; *19*). These data are consistent with a role for PLS in a number of
143 ethylene responses and other related signalling, stress and developmental processes.
144 To understand better the relationship between PLS peptide structure and function, and
145 to investigate conservation of PLS function between species, we carried out synthetic peptide
146 feeding experiments using hydroponically grown seedlings. The *Arabidopsis* relative *Camelina*
147 *sativa* contains a gene with partial sequence identity to the *Arabidopsis PLS* gene, encoding a
148 predicted peptide sequence that is 22 amino acids long and identical to the N-terminal 22 amino
149 acids of the *Arabidopsis* PLS except for a phenylalanine to serine substitution at position nine
150 (Fig. 1a). We synthesized full-length PLS peptide, PLS(FL) and truncated versions from both
151 *Arabidopsis* and *C. sativa* (Fig. 1a) and supplied the peptides to *Arabidopsis pls* mutant seedlings
152 hydroponically. The full-length peptides from both *Arabidopsis* and *C. sativa* and the N-terminal
153 22 amino acids sequence of the *Arabidopsis* peptide (N1) were each able to rescue the short
154 primary root length of the *Arabidopsis pls* mutant (Figs. 1d), similar to transgenic overexpression
155 and genetic complementation using the wild type PLS coding sequence (*14, 19*). The mean
156 primary root length of wild type (C24) seedlings did not change across all peptide treatments,
157 while supply of *pls* seedlings with 50 nM PLS(FL) and N1 peptides showed a rescue of root
158 growth (Fig. 1e), and *t*-tests showed there was no significant difference between the rescue effects
159 of PLS(FL) and PLS(N1); $P > 0.1$, n = 25). However, neither a 9 amino acids sequence (N2, Fig.
160 1e) from the N-terminus, nor C-terminal sequences of 14 (C1) or 24 (C2) amino acids from
161 *Arabidopsis* PLS were able to rescue the mutant (Fig. 1e); each of these shorter peptides lacks
162 one of the two Cys residues found in the functional longer length peptides PLS(FL) and PLS(N1).
163 Imaging showed that a fluorescent tagged (5-carboxyfluorescein, 5-FAM) version of the
164 *Arabidopsis* N-terminal 22 amino acids sequence of the peptide (N1) is taken up by the roots,
165 and also rescues the mutant root phenotype (Fig. S3a,b).
166
167 **PLS localizes to the cytosolic side of the endoplasmic reticulum**
168 Since genetic studies suggest that PLS acts close to the ethylene receptor (*18*), we hypothesized
169 that it should localize to the same subcellular compartment. The ethylene receptor in *Arabidopsis*
170 is localized to the ER (*12*), and a *proPLS::PLS:GFP*-generated fusion protein (PLS:GFP) was
171 found to co-localize with both the ER marker dye ER-Tracker™ (Fig. 2a-c) and with an ER-
172 targeted red fluorescent protein RFP-HDEL (*24*) in transgenic plants (Fig. 2g-i). PLS:GFP also
173 appears to localize to the nucleus and cytoplasm (Fig. 2). As controls, free GFP protein expressed
174 under the control of the *PLS* promoter is not co-localized to the ER (Fig. 2d-f) and, as expected,
175 the Golgi marker SH:GFP does not co-localize with ER Tracker (Fig. 2m-o). *Trans*-Golgi-
176 localized SULFOTRANSFERASE1 (ST1) mCherry (*25*) visualization shows PLS:GFP does not
177 localize to the Golgi (Fig. 2j-l). To further clarify the side of the ER membrane on which PLS
178 localizes, transient expression of redox-sensitive GFP (roGFP2) fusions of PLS were carried out.
179 The different excitation properties of roGFP2 in an oxidizing (ER lumen) or reducing
180 environment (cytosol) allows discrimination of the precise location of PLS fused to RoGFP2.
181 Ratiometric analysis and comparison with proteins of known localization (i.e. cytosolic RoGFP2,
182 ER luminal RoGFP2, cytosolic v-SNARE SEC22-GFP, ER luminal RoGFP2-SEC22; *26*)
183 revealed that PLS as either an N- or C-terminal roGFP2 fusion resides at the cytosolic side of the
184 ER and is not localized in the ER lumen (Fig. 2p).
185
186 **PLS interacts with the ethylene receptor protein ETR1**
187 We hypothesized that PLS plays a role in receptor function and investigated whether this
188 involved direct interaction with the receptor complex. Preliminary experiments using yeast 2-
189 hybrid analysis suggested that PLS interacts with ETR1 (Fig. S4). Confirmation of the physical

190 interaction between PLS and ETR1 in plants came from co-immunoprecipitation (Co-IP) analysis.
191 *Agrobacterium* containing a plasmid encoding PLS linked to a C-terminal GFP and ETR1 with
192 a C-terminal HA tag was infiltrated into *Nicotiana benthamiana* leaves for transient expression.
193 After 3 d, interaction was confirmed by western blotting after Co-IP with either anti-GFP beads
194 (showing PLS pulls down ETR1) or anti-HA beads (showing ETR1 pulls down PLS) (Fig. 3a).
195 GFP-only controls did not show binding with ETR1, demonstrating the interaction is dependent
196 on the presence of the PLS peptide. The addition of 0.5 μM copper sulphate to the protein extract
197 used for Co-IP experiments stabilized the PLS-ETR1 interaction. The presence of copper ions
198 resulted in almost 3-fold more PLS:GFP detected upon pulldowns with ETR1-HA, or conversely
199 of ETR1-HA pulled down with PLS-GFP, compared to the same assay in the presence of the
200 metal chelator 2 mM EDTA (Fig. 3a, b).
201 To investigate the specificity of PLS binding, synthetic full length PLS peptide PLS(FL)
202 was introduced into the infiltrated *N. benthamiana* leaves 30 min before the tissue was harvested.
203 The addition of 25 nM synthetic PLS caused a ca. 80% reduction in PLS-GFP binding to ETR1-
204 HA (Fig. 3c, d), suggesting that the synthetic PLS peptide competes for ETR1 binding, and
205 showing the specificity of PLS for ETR1. Interestingly, the anti-GFP beads bound two sizes of
206 PLS-GFP protein (Fig. 3e), both of which were larger than a GFP-only control, suggesting that
207 the PLS peptide undergoes cleavage, a change in conformation, post-translational modification
208 or incomplete reduction of Cys residues on some PLS. When using ETR1-HA to pull down PLS-
209 GFP, only the larger peptide was present (Fig. 3e, f), suggesting that ETR1 binds the full length
210 PLS peptide, but that PLS may be modified after ETR1 binding.
211 To pinpoint the interaction site at the receptor in more detail, *in vitro* binding studies
212 were performed with purified receptor variants and PLS by microscale thermophoresis (MST;
213 Fig. 3g). Binding of PLS was observed only with receptor variants containing the N-terminal
214 transmembrane domain (TMD). In contrast, no binding was detected with ETR1 lacking this
215 domain ($ETR1^{306-738}$). The TMD harbors the ethylene and copper binding region (*27*).
216
217 **PLS binds Cu(I) and forms protein-protein interactions with copper chaperones ATX and**
218 **CCH and with RAN1**
219 Cysteine residues are common metal-ligand binding residues in low molecular weight copper-
220 handling peptides, and predictions of PLS structure suggests a single α-helix plus unstructured
221 region with two cysteines ($CX_{10}C$ arrangement where X is any amino acid), with some analogy
222 to copper-metallochaperones such as Cox17 or other CX_9C twin proteins (*28*). In view of both
223 structural considerations and the copper-dependency of ETR1 we determined whether the two
224 cysteine residues (C6 and C17) in PLS play a functional role, namely in *pls* mutant
225 complementation and in copper binding. A mutated *Arabidopsis* full-length peptide in which
226 both cysteines were replaced with serine, PLS(FL C6S, C17S), was non-functional in hydroponic
227 root feeding assays (Fig. 4a). Furthermore, as indicated above, the 9 amino acids sequence N2
228 and C-terminal sequences C1 and C2 from *Arabidopsis* PLS, which each contain only one
229 cysteine residue, were unable to rescue the mutant (Fig. 1e). These results indicate the
230 requirement of the two cysteine residues for biological activity. Interestingly, RNA-seq data
231 showed that nineteen out of 287 genes associated with response to metal ion (GO:0010038) were
232 also down-regulated in the *pls* mutant (Table S4, Fig. S2b, enrichment *FDR = 0.000057*; *20*).
233 To determine a possible role for PLS and the cysteine residues in binding Cu(I),
234 synthesised PLS peptide (44.8 μM) was titrated with Cu(I) ions under strictly anaerobic conditions
235 and monitored for copper-dependent spectral features. Both UV-vis (putative metal-to-ligand
236 charge-transfer) and fluorescence (putative tyrosine solvent access) spectra of PLS changed as a
237 function of Cu(I) ion concentration, consistent with complex-formation (Fig. 4b,c). The inflection

238 in the UV-vis data at ca. 20 μM and the absence of further quenching in the fluorescence data
239 above ca. 22 μM suggest that PLS binds Cu(I) ions in a 2:1 stoichiometry (Figs. 4b). We further
240 titrated PLS peptide against bicinchoninic acid (BCA), which is a chromophore that binds Cu(I)
241 (*29*) (Fig. 4c). The rationale was to determine whether PLS could compete Cu(I) from BCA,
242 indicative of binding by PLS. PLS peptide was titrated with Cu(I) in the presence of 87 μM BCA.
243 In the presence of the PLS peptide (44.8 μM), the concentration of Cu(I) required to saturate BCA
244 increased by ca. 20 μM, and the initial gradient is shallower than in the control (Figs. 4c,d, S5).
245 Thus PLS withholds Cu(I) from BCA, implying an affinity for Cu(I) (K_{Cu} PLS) within an order of
246 magnitude of K_{Cu} of BCA, and these data also provide further support for a 2:1 stoichiometry of
247 binding. Titration experiments also show that synthetic PLS(FL) withholds Cu(I) from BCA (Fig.
248 S6), but the mutant PLS (FL C6S, C17S) does not (Fig. S7), confirming a role for those cysteine
249 residues in Cu(I) binding. As an additional and complementary strategy, to eliminate potential
250 solubility problems of PLS in determining accurately the stoichiometry and affinity for Cu(I)
251 (these studies require complete solubility for precise affinity quantification), we also tested a PLS
252 fusion to maltose binding protein (MBP-PLS) which was found to retain solubility when titrated
253 with Cu(I) ions under strictly anaerobic conditions. MBP-PLS (14 μM) was found to withhold ca.
254 7 μM Cu(I) from BCA, indicative of a 2:1 PLS:Cu(I) stoichiometry, and tight binding is cysteine-
255 dependent (Fig. 4e). A β_2 affinity of 3.79 (±1.5) x10^{19} M^{-2} was determined by competition against
256 an excess of BCA, and the fit significantly departs from simulations 10x tighter or weaker (Fig.
257 4f, Fig. S8).
258 Metal binding in biology is challenging to predict because the formation of metal-
259 protein complexes is a combined function of metal affinity for a given protein and metal
260 availability, which would need to be known for Cu(I) in the *Arabidopsis* cytosol in the case of
261 PLS (Fig. 2p). Cu(I) occupancy of the cytosolic copper chaperone ANTIOXIDANT PROTEIN
262 1 (ATX1) tracks with fluctuations in available cytosolic Cu(I) such that its affinity approximates
263 to the mid-point of the range of Cu(I) availabilities within this eukaryotic compartment (*30, 31*).
264 *Arabidopsis* ATX1 was therefore expressed and purified to determine a 1:1 ATX1:Cu(I)
265 stoichiometry and affinity $K_{D\ Cu(I)}$ of 5.47 (±0.6) x10^{-18} M (Fig. 4g inset, Fig. S9). Figure 4f
266 reveals that the cytosolic concentration of PLS would need to exceed (improbable) millimolar
267 concentrations for Cu(I)-dependent homodimers to form at this cytosolic Cu(I) availability
268 (mathematical models and equations shown in Supplementary text). It is thus unlikely that the
269 Cu(I):PLS_2 complex alone delivers Cu(I) to interacting cuproprotein ETR1. Cu(I)-dependent
270 PLS heterodimeric complexes are the more likely functional species.
271 To investigate possible interaction between PLS and RAN1, PLS was titrated against
272 fluorescently labelled RAN1 and RAN1 truncation mutants for comparison. RAN1, NterRAN1
273 and CterRAN1 (DeltaRAN1 in Fig. 4h) were purified and labelled as described (*17*). NterRAN1
274 is a truncation containing only the two N-terminal metal-binding-domains, whereas CterRAN1
275 is a construct lacking this region. Using MST, direct interaction was observed between PLS and
276 RAN1. Dissociation constants indicate that PLS interacts predominantly with the N-terminal
277 metal-binding-domains, but only weakly with the C-terminal region (Fig. 4h). Moreover, the
278 soluble copper chaperones ATX1 and CCH also interact with PLS. Titration experiments were
279 carried out with fluorescently labelled copper chaperones ATX1, CCH and CCHΔ, a mutant
280 lacking the plant specific C-terminal extension; though the C-terminus on its own (DeltaN) is not
281 soluble and can thus not be checked for interaction with PLS. PLS interacts with these soluble
282 copper chaperones at similar affinity as obtained for RAN1 (Fig. 4i). Of relevance here is the
283 observation that ATX1 interacts directly with RAN1 to deliver copper at the ER (*32*). Cu(I)-
284 dependent PLS heterodimeric complexes may therefore modulate multiple cuproproteins in the
285 Cu(I)ETR1 maturation pathway.

Discussion

We present evidence of a role for the PLS peptide as a regulator of ethylene receptor function. Peptides can act as ligands for receptor kinases to regulate signalling pathways, such as in plant immunity (*33*), development (*34*) or in response to abiotic stresses (*35*). We propose that the PLS peptide regulates the ethylene receptor by a different mechanism, i.e. not as a ligand (which for ETR1 is the hormone ethylene) but as part of the metalation mechanism for Cu(I) delivery to the receptor, a process essential for ethylene binding (*10*). Given that PLS is expressed in specific cell types (*19*) it seems likely that PLS adds a level of regulation of receptor function in specific tissues, and most obviously in the root tip. While PLS:GFP localizes to several subcellular compartments including cytoplasm and nucleus, some localizes to the ER where the ethylene receptor is found (Fig. 2). Furthermore we demonstrate that PLS can interact directly with the receptor protein ETR1 (and specifically with the N-terminal copper-binding domains of ETR1), with the Cu-transporting P-type ATPase RAN1, and with two Cu chaperones, ATX1 and CCH. ATX1 and CCH have also previously been shown to bind RAN1 (*32*).

Many plant peptides involved in signalling are processed from longer pre-proteins (*36*). In contrast, PLS is translated from an open reading frame to produce a functional 36 amino acids peptide; the full-length peptide appears to be cleaved or otherwise modified on binding to ETR1 (Fig. 3e). It is possible that the three arginines (amino acids 10-12) may represent a cleavage site (*37, 38*) which would produce the observed shorter GFP fusion protein detected in co-IP experiments (Fig. 3e). The size of the PLS-GFP cleavage product (ca. 30 kD) suggests that this peptide fragment represents GFP (ca. 27 kDa) plus a 3 kDa fragment of the C-terminal region of PLS. Such cleavage would likely inactivate PLS function as we demonstrate that shorter N- and C-terminal fragments (each with only one cysteine residue) are not biologically active (Fig. 1e). Such cleavage might represent a mechanism by which PLS releases Cu(I) to the receptor or to other interacting Cu(I)-transporting proteins RAN1, ATX1 and/or CCH.

Previously there has been proposed a model for copper delivery into the cell via the plasma membrane-located HMA5 transporter to RAN1 via ATX1 and/or CCH (*18*, *32*). Arabidopsis has three known copper chaperones, ATX1, CCH and a Cu chaperone for superoxide dismutase CCS (*39, 40, 41*). These are required for copper homeostasis, and both ATX1 and CCH have been shown to interact with RAN1, providing a link with ethylene signalling (*41, 42*). Chaperones are required for the transport of reactive copper to the correct compartment via these chaperones, avoiding cytotoxicity, following import into the cell via copper transporters such as COPT1 and HMA5; the latter being structurally similar to RAN1 (*43, 44*). Loss of function mutants *cch* and *atx1* have no abnormal phenotype when grown under standard conditions, but the *atx1* and the *atx1 cch* double mutant, though not the *cch* single mutant, are hypersensitive to exogenous Cu (*45*). ATX1 and CCH functions have likely diverged, a view supported by their differential transcriptional regulation by copper and different cell type specificities (*45*). The *ran1* mutant is however not copper-hypersensitive, while *hma5* is; and the *pls* mutant is, like *ran1*, not copper hypersensitive (Fig. S10), indicative of a role that is distinct from that of ATX1 or CCH. The ATX1 interaction with RAN1 is indicative of its role in copper transport from the cell surface to internal targets, including RAN1 and potentially to PLS.

We propose that PLS represents a new component of this pathway, providing some tissue-specificity to the Cu(I) delivery process. Given the low probability that PLS would act as a copper chaperone directly due to its predicted low concentration in the cell (Figs. 4f, S8), it more likely partners with an existing chaperone such as ATX1 or CCH close to the ER, which would provide a concentrating effect, facilitating Cu(I) delivery to RAN1 and ETR1. In this

333 scenario, a down-regulation of *PLS* expression or loss-of-function mutation of the *PLS* gene
334 would lead to a depletion of correctly coordinated Cu(I) at the receptor through reduced
335 intermediate PLS heterodimer formation with ATX1 and/or CCH and ultimately RAN1, in turn
336 leading to a non-functional receptor that cannot activate CTR1. This would be expected to
337 promote ethylene signaling, consistent with the observed effect of ACC treatment on reducing
338 *PLS* expression and enhancing ethylene responses (Fig. S11). A functional PLS complex may be
339 removed from ETR1 by the observed cleavage or modification of PLS. Future structural studies
340 should reveal more about the PLS-ETR1-RAN1-chaperone interaction and role of copper ions in
341 ethylene signal transduction, which represents a new paradigm for the regulation of signaling
342 protein function by metals.
343 While the *pls* mutant shows evidence for a role of PLS in ethylene signalling, the
344 relationship is not simple. For example, the *PLS* overexpresser is not completely insensitive to
345 the ethylene precursor 1-aminocyclopropane-1-carboxylate (ACC) and does not completely
346 suppress the *ctr1* mutation (*14*), suggesting some distinct function compared with other
347 regulatory components. The *pls* mutant shares (statistically significant) overlap in DEGs with the
348 *ctr1* mutant, whereby 11.9% of the *ctr1* DEGs are shared with *pls* (each compared to the
349 respective wild types; Fig. S12). We have also shown in other previous work that there is
350 crosstalk between PLS, ethylene and other signalling pathways, notably auxin, cytokinin and
351 ABA (e.g. *21, 22, 23*), and observed 'leakiness' of the *PLS* overexpression ethylene phenotype,
352 and distinctiveness of *pls* compared to other ethylene signaling mutants, may be linked to its
353 restricted expression pattern. The root tip, where *PLS* is most strongly expressed, is a site of high
354 auxin, whereby an auxin concentration maximum is formed around the stem cell niche to regulate
355 both stem cell identity and function (*46*). Auxin can induce ethylene biosynthesis by upregulation
356 of the ethylene biosynthetic enzyme ACC synthase (*47*), and high ethylene concentrations can
357 lead to both reduced meristem function and aberrant division of the quiescent centre and cells
358 within the stem cell niche and columella (*48*). Therefore ethylene biosynthesis and signalling in
359 the root tip must be tightly regulated to allow growth control. *PLS* expression is transcriptionally
360 activated by auxin and suppressed by ethylene, together forming a signaling network with
361 cytokinin, also produced in the root tip, to regulate ethylene responses and root growth. This
362 network provides a mechanism to suppress growth-inhibitory ethylene responses in the high
363 auxin environment of the root tip, which is dependent on the tissue-specific expression of *PLS*
364 (*21*) (Fig. S11) and is mediated through ethylene receptor metalation.
365
366

367 # Methods

368 **Plant Material**

369 Seedlings of *Arabidopsis thaliana* ecotype either C24 or Col-0, or *pls* mutants or transgenic *PLS*
370 overexpressers, all from lab stocks, were grown on solid sterile half-strength MS10 medium on
371 2.5% Phytagel (Sigma-Aldrich) in 90 mm Petri dishes (Sarstedt, Leicester, UK) at 21°C, under
372 a 16 hour photoperiod as described (*14, 19*). *Nicotiana benthamiana* plants (lab stocks) were
373 grown in a controlled environment (21°C, 16 h photoperiod) for transient expression studies in
374 leaf tissue. For hydroponic feeding studies, *Arabidopsis* seedlings were cultured in liquid
375 medium (1 ml/well) in sterile 24-well plates (Sarstedt), essentially as described (*49*). For
376 hormone and peptide assays, one seedling was grown in each well, at 21°C, under a 16 h
377 photoperiod. For peptide feeding experiments, purified freeze-dried peptide was dissolved in
378 DMSO to create a 500 µM stock solution. Peptide stock solution was added to liquid ½ MS10
379 plant media containing 0.1% DMSO to make a final peptide concentration of 50 or 100 nM (or

380 10, 25, 50 and 100 nM for dose-dependent assays). For copper treatments, 1 mM $CuSO_4$ solution
381 was filter-sterilized and added to autoclaved liquid ½ MS10 plant media to create final $CuSO_4$
382 concentrations of 0, 5, 10, 15, 20, 25, 30, 35, 40, 45 and 50 µM. The copper chelator
383 bathocuproine disulphonic acid (BCS) was added to liquid medium to produce final
384 concentrations of 0, 10, 50, 100, 250 and 500 µM. Seedlings were scanned to create a digital
385 image and root lengths of seedlings were measured using ImageJ. Statistical analysis was
386 performed using the Real Statistics Resource Pack software (Release 3.8, www.real-
387 statistics.com) in Excel (Microsoft).
388
389 **Peptide Synthesis**
390 Peptides were either obtained from Cambridge Research Biochemicals (Billingham, UK) or
391 synthesized in the laboratory by Fmoc solid phase peptide synthesis (SPPS) on a CEM Liberty1
392 single-channel peptide synthesiser equipped with a Discover microwave unit. Reactions were
393 performed in a 30 ml PTFE reaction vessel with microwave heating and agitation by bubbling
394 nitrogen. Peptide synthesis was carried out using 2-chlorotrityl chloride resin (0.122 mmol g^{-1},
395 Novabiochem) using Fmoc-protected amino acids. The first amino acid residue at the C-terminus
396 (histidine) was coupled manually by mixing 76 mg (1 eq.) Fmoc-His(Trt)-OH, 0.09 ml (4 eq.)
397 *N,N*-diisopropylethylamine (DIPEA), 1 ml dichloromethane (DCM) and 1 ml
398 dimethylformamide (DMF) until the amino acid powder had dissolved. The mixture was added
399 to 0.1 mmol resin and stirred gently for 120 minutes at room temperature. Resin was washed
400 with 3x DCM/MeOH/DIPEA (17:2:1), 3x DCM, 2x DMF and 2x DCM. Amino acid coupling
401 reactions were performed using Fmoc-protected amino acids present in a 5-fold excess (2 M
402 concentration), HOBt (0.5 M HOBt in DMF, used at the activator position) and DIC (0.8 M in
403 DMSO, used at the activator base position). For double and triple couplings the reaction vessel
404 was drained after each coupling cycle and fresh reagents were added. Before each coupling, a
405 room temperature preactivation period of 1 to 2 hours was used. Microwave-assisted couplings
406 were performed for 10 minutes at 75°C at 25W power. Cys and His residues were coupled at low
407 temperature (10 minutes at room temperature followed by 10 minutes at 50°C, 25W). Arg
408 residues were double coupled, firstly by 45 minutes at room temperature plus 5 minutes at 75°C
409 (25W), and second by the standard microwave conditions above. Fmoc group removal was
410 carried out by two piperidine solution treatments (20% piperidine in DMF) in succession: 5
411 minutes then 10 minutes. Peptide cleavage from resin was carried out in 3 ml 95% TFA in dH^-
412 $_2O$/TIPS (2.85 ml TFA, 0.15 ml dH_2O, 0.15 ml triisopropylsilane). Peptide was dissolved in water
413 with a small volume of MeCN and lyophilized to produce a powder using a Christ ALPHA 1-2
414 LD_{plus} freeze dryer.
415
416 **Preparative High-Performance Liquid Chromatography (HPLC)**
417 Peptide products were analysed and purified by HPLC at 280 nm. 25-50 mg of freeze-dried
418 peptide sample was dissolved in 1 ml 1:1 H_2O:MeCN and injected onto a Speck and Burke
419 Analytical C18 Column (5.0 µm, 10.0 x 250 mm) attached to a PerkinElmer (Massachusetts,
420 USA) Series 200 LC Pump and 785A UV/Vis Detector. Separation was achieved by gradient
421 elution of 10-80% solvent B (solvent A = 0.08% TFA in water; solvent B = 0.08% TFA in ACN)
422 over 60 minutes, followed by 80-100% B over 10 minutes, with a flow rate of 2 ml/min. Selected
423 peptide fractions were lyophilized and a mass assigned using MALDI-TOF MS. Peptide
424 sequences were identified using MALDI-TOF MS, using an Autoflex II ToF/ToF mass
425 spectrometer (Bruker Daltonik GmBH, Germany) equipped with a 337 nm nitrogen laser. MS
426 data was processed using FlexAnalysis 2.0 (Bruker Daltonik GmBH).
427

428 **Imaging**
429 CSLM images were obtained by a Leica SP5 TCS confocal microscope using 40X and 63X oil
430 immersion lenses. For propidium iodide staining, whole *Arabidopsis* seedlings were incubated
431 in 10 mg/l propidium iodide solution for 90 s. *pPLS::PLS:GFP, pPLS::GFP* and *p35S::GFP*
432 seedlings were grown for 7 d on Phytagel ½ MS10 medium before ca. 25 mm of the root tip was
433 removed and mounted in dH_2O on a microscope slide, and a 1.5 mm cover slip was placed on
434 top prior to imaging. The ER marker *p35S::RFP:HDEL* (*24*) (kindly provided by Dr. Pengwei
435 Wang, Durham University), and the trans-Golgi apparatus marker *pFGC-ST:mCherry* (obtained
436 from Nottingham Arabidopsis Stock Centre, www.arabidopsis.info) were introduced into
437 *pPLS::PLS:GFP* plants by the floral dip method of transformation (*50*) using *A. tumefaciens*
438 GV3 101. ER was also localized using ER Tracker™ Red (Life Technologies). Seven day-old
439 seedlings were stained for 30 min in the dark in liquid ½ MS10 media containing 1 µM ER
440 Tracker™ Red.
441
442 **RNA Isolation, RNA Sequencing, RT-qPCR**
443 RNA was extracted from 7 day-old seedlings grown on half strength MS10 medium using the
444 Sigma-Aldrich Plant Total RNA Kit (STRN50) and the On-Column DNase I Digestion Set
445 (DNASE10-1SET), essentially as described (*51*). Tissue was ground in liquid nitrogen before
446 incubation in lysis solution containing 2-mercaptoethanol at 65°C for 3 min. Debris was removed
447 by centrifugation and column filtration and RNA was captured onto a binding column using the
448 supplied binding solution. DNA was removed by wash solutions and DNase treatment on the
449 column. Purified RNA was eluted using RNAase free water.
450 The Illumina HiSeq 2500 System was used for RNA sequencing of three biological
451 replicate samples, with libraries prepared using the Illumina TruSeq Stranded Total RNA with
452 Ribo-Zero Plant Sample Preparation kit (RS-122-2401), essentially as described (*51*).
453 Ribosomal RNA (rRNA) was removed and purified RNA was quality checked using a
454 TapeStation 2200 (Agilent Technology) with High Sensitivity RNA ScreenTape (5067-5579).
455 mRNA was fragmented into 120-200 bp sequences with a median size of 150 bp and used
456 as template to synthesize first strand cDNA using reverse transcriptase and random primers,
457 followed by second strand cDNA synthesis with DNA Polymerase I and RNase H. Newly
458 synthesized cDNA had a single adenine base added with ligation of adaptors, before being
459 purified and amplified by PCR to make the final library. Library quality control was carried out
460 again using a TapeStation with D1000 ScreenTape (catalog number 5067-5582). RNA-seq data
461 were aligned to the TAIR10 (EnsemblePlants, release 58) genome sequence with corresponding
462 gtf file using STAR (v 2.7.11a; *52*) to obtain read count per gene. Read count per gene was
463 analysed using DESeq2 v 1.40.2 (*53*) to get p values, adjusted p values, and log2 fold changes.
464 Differentially expressed genes (DEGs) were identified with the criteria of adjusted p value <
465 0.05. Gene ontology analysis was performed using AgriGO (*54*) singular enrichment analysis.
466 Gene expression heatmaps were generated from log2 normalized counts using pheatmap
467 (v1.0.12, https://cran.r-project.org/web/packages/pheatmap/index.html) with row scaling.
468 RNA-seq data were deposited in GEO (https://www.ncbi.nlm.nih.gov/geo/) with accession
469 number GSE256166 (*20*).
470 For RT-qPCR, RNA was extracted from 7 day-old seedlings (3 biological replicates, 20
471 mg of tissue) as described (*51*). Total mRNA was extracted using Dynabeads®mRNA DIRECT™
472 kit with Oligo$(dT)_{25}$ labelled magnetic beads. cDNA was prepared using a SuperScript®IV First-
473 Strand synthesis system. Samples were checked for the presence of genomic DNA by PCR with
474 *ACTIN2* primers ACT2 forward and reverse. Primer sequences were determined using Primer-
475 BLAST (https://www.ncbi.nlm.nih.gov/tools/primer-blast/). Primers are listed in Table S7.

476
477 **Protein-protein interaction studies**
478 **Yeast 2-hybrid**
479 The GAL4 two-hybrid phagemid vector system was used to detect protein-protein interactions
480 *in vivo* in yeast, using the reporter genes β-galactosidase *(lacZ)* and histidine (*HIS3*) in the YRG-
481 2 yeast strain, essentially as described (*55*). DNA that encodes the target (ETR1) and bait (PLS)
482 was inserted into the pAD-GAL4-2.1 A and pBD-GAL4 Cam phagemid vectors respectively and
483 expressed as hybrid protein. The hybrid proteins were then assayed for protein-protein
484 interaction.
485 DNA encoding the target and bait proteins were prepared by PCR amplification using
486 primer designed the specifically for the DNA encoding the target (ETR1) and bait (PLS). Each
487 set of primer contained specific endonucleases on the ends of primer corresponding to the
488 endonucleases in the MCS of pAD-GAL4-2.1 A and pBD-GAL4 Cam phagemid vectors. The
489 DNA construct of the target (ETR1) and bait (PLS) with specific restriction sites on the ends was
490 then transformed into the TOPO 2.1 vector to check the sequence of the amplified DNA by
491 sequencing with M13 forward (CTG GCC GTC GTT TTA C) and M13 reverse (CAG GAA
492 ACA GCT ATG AC). The two vectors, pAD-GAL4-2.1 and pBD-GAL4 Cam were digested
493 using specific restriction endonucleases and dephosphorylated prior to ligating the insert DNA.
494 The DNA encoding the target (ETR1) and bait (PLS) was then ligated into the same reading
495 frame as the GAL4 AD of the pAD-GAL4-2.1 phagemid vector and the GAL4 BD of the pBD-
496 GAL4 Cam phagemid vector.
497 The following primers were used for PCR amplification:
498 ETR1:
499 Forward primer GAA TCC ATG GAA GTC TGC AAT TGT A (Eco RI on 5' end)
500 Reverse primer GTC GAC TTA CAT GCC CTC GTA CA (Sal I on 5'end)
501 PLS:
502 Forward primer CTG GAG ATG AAA CCC AGA CTT TGT (Xho I on 5' end)
503 Reverse primer GTC GAC ATG GAT TTT AAA AAG TTT (Sal I on 5' end)
504 The pGAL4 control plasmid was used alone to verify that induction of the *lacZ* and
505 *HIS3* genes has occurred and that the gene products are detectable in the assay used. The pLamin
506 C control plasmid was used in pairwise combination with the pAD-WT control plasmid or with
507 the pAD-MUT control plasmid to verify that the *lacZ* and *HIS3* genes are not induced as the
508 protein expressed by each of these pairs do not interact *in vivo*.
509 The control plasmids were transformed into the YRG-2 strain prior to the initial
510 transformation of the bait and the target plasmids. The control plasmids were used separately or
511 in pairwise combination in the transformation of the YRG-2 yeast strain. The yeast competent
512 cells were cotransformed with the bait and target plasmids by sequential transformation. First,
513 yeast were transformed with the bait plasmid and assayed for expression of reporter genes.
514 Second, yeast competent cells containing the bait were prepared and transformed with the target
515 plasmid.
516
517 **Bimolecular fluorescence complementation analysis (BiFC)**
518 BiFC was carried out essentially as described previously (*56*). Full-length *Arabidopsis ETR1* and
519 *PLS* cDNA sequences were cloned respectively into the vectors *pDH51-GWYFPn* (AM779183,
520 to form *ETR1-YFPn*) and *pDH51-GW-YFPc* (AM779184, to form *PLS-YFPc*), and the *CTR1*
521 cDNA was cloned into *pDH51-GW-YFPc* (*CTR1c*), as a control for ETR1 interactions. Intact
522 YFP plasmid was also used as a positive control and YFPc alone was used as a negative control
523 as described previously (*57*). Plasmids were kindly provided by Prof. Don Grierson, University

524 of Nottingham. Transient expression studies following microprojectile bombardment on onion
525 cells. Plasmids were adhered to gold particles to make gold-coated cartridges. 5-10 of these
526 cartridges were used for bombarding onion peel cells. Agar plates containing bombarded onion
527 peels were incubated for 8 hours in dark and then a 1 cm section of the peel was stained with
528 propidium iodide (10 mg/ml) for 1 min and viewed under confocal microscope. Experiments
529 were repeated at least three times.
530
531 **Co-immunoprecipitation**
532 To investigate the interaction between the PLS peptide and the ethylene receptor ETR1, two
533 DNA constructs were created by Gateway cloning. The 105-nucleotide *PLS* gene (without the
534 stop codon) was inserted into the pEarlyGate103 (pEG103) destination vector, containing the
535 *p35S* promoter and a C-terminal GFP tag, producing a vector containing the *p35S::PLS:GFP*
536 DNA. The ETR1 cDNA was inserted into the pEarlyGate301 (pEG301) vector to create a
537 *p35S::ETR1:HA* construct, producing an ETR1 protein with a C-terminal HA tag.
538
539 **Infiltration into *Nicotiana benthamiana***
540 The transient expression of constructs in *Nicotiana benthamiana* (tobacco) leaves was based on
541 a previously published method (*57*). Experiments were replicated up to 5 times. Competent
542 *Agrobacterium tumefaciens* GV3101 cells were transformed with the desired plasmid containing
543 the gene of interest. Individual colonies were used to inoculate liquid LB cultures containing 25
544 µg/ml gentamicin, 50 µg/ml rifampicin and the specific antibiotic required to select for the
545 desired plasmid. The liquid cultures were grown at 28°C for 14-16 h with shaking at 220 rpm.
546 Additionally, liquid cultures of GV3101 containing the p19 protein that is encoded by the tomato
547 bushy plant virus were also prepared in order to suppress post-transcriptional gene silencing (*57*).
548 The overnight cultures were grown until an OD_{600} of approximately 0.6 was reached, and then
549 centrifuged at 3000 x *g* for 5 min. These cells were then twice washed with 10 ml of an infiltration
550 buffer containing 10 mM $MgCl_2.6H_20$, resuspended in 1 ml of the same solution and
551 subsequently incubated at room temperature for 3-5 h. Prior to infiltration, each construct was
552 mixed with p19 and infiltration buffer in a 1:1.2:1.8 ratio.
553 Several small cuts were made with a scalpel on the abaxial surface of the *N.*
554 *benthamiana* leaves and were subsequently injected with each of the constructs using a syringe.
555 The plants were approximately 7 to 10 weeks old; the chosen leaves were healthy and of length
556 3-6 cm, and 3 to 4 leaves were infiltrated with each construct.
557
558 **Protein extraction and PLS/ETR1 co-immunoprecipitation**
559 Total protein was extracted from the infiltrated leaves of *N. benthamiana* plants 3 d after
560 infiltration for co-immunoprecipitation (co-IP/pull-down) experiments to investigate the
561 interaction between PLS and ETR1 proteins.
562 1.5 g of leaf tissue was harvested from each *A. tumefaciens* construct infiltration event,
563 frozen with liquid nitrogen and ground gently using a mortar and pestle. For competition assays,
564 5 nM or 25 nM full-length PLS peptide was also infiltrated in the presence of 50 µM MG-132 (a
565 proteasome inhibitor) 30 min prior to tissue freezing. The homogenate was transferred to a pre-
566 cooled microcentrifuge tube. 2 ml of extraction buffer was added (20 mM sodium phosphate pH
567 7.4, 100 mM NaCl, 80 mM KCl, 1% glycerol, 0.1 % Triton, 10 mM DTT, plus 1 mini protease
568 inhibitor cocktail tablet, Roche, Switzerland) per 20 ml of extraction buffer, and the extra
569 addition of either 2 mM EDTA or 0.5 µM $CuSO_4$ for binding studies), and the solution was
570 ground further and vortexed until the homogenate was smooth. The solution was centrifuged for
571 12 min at 14000 x *g*, 4°C.

572 ChromoTek (Planegg, Germany) anti-GFP beads were used to immunoprecipitate the
573 PLS-GFP protein, and Sigma-Aldrich (St. Louis, USA) anti-HA beads for the HA-tagged ETR1.
574 25 µl bead slurry was resuspended in 500 µl ice-cold dilution buffer (20 mM sodium phosphate
575 pH 7.4, 100 mM NaCl, 80 mM KCl, 1% glycerol, 0.1 % Triton, 10 mM DTT, plus 1 mini protease
576 inhibitor cocktail tablet) and centrifuged for 2 minutes at 2500 x *g* at 4°C. The supernatant was
577 discarded and the beads were washed twice more with 500 µl ice-cold dilution buffer.
578 The supernatant from the protein sample extraction from *N. benthamiana* plants was
579 mixed with 50 µl GFP beads or HA beads and incubated for 30 minutes at 4°C, mixing every 2
580 minutes. The mixture was centrifuged at 2500 x *g* for 2 min at 4°C, washed twice with 500 µl
581 ice-cold dilution buffer, and the beads were transferred to a new microcentrifuge tube. The target
582 protein was eluted with the addition of 100 µl 2x SDS sample buffer (120 mM Tris pH 6.8, 50
583 mM 4% (w/v) SDS, 20% (v/v) glycerol) and the sample was boiled for 10 minutes at 95°C to
584 dissociate immunocomplexes from the beads. The mixture was centrifuged for at 2500 x *g* for 2
585 minutes at 4°C to separate the beads, and the supernatant was transferred to a new
586 microcentrifuge tube. The supernatant was used in SDS-PAGE analysis.
587
588 **Sodium Dodecyl Sulphate Polyacrylamide Gel Electrophoresis (SDS-PAGE)**
589 SDS-PAGE was used to separate protein fragments. The complexed proteins from the pull-down
590 assay were analysed on 10-12% acrylamide gels.
591 Firstly, the resolving gel was prepared by adding the chosen amount of acrylamide
592 (ProtoGel, 30% (w/v) acrylamide, 0.8% (w/v) bisacrylamide solution, National Diagnostics) to
593 the resolving buffer (0.1% (w/v) SDS, 375 mM Tris, polymerized via the addition of 0.1% (v/v)
594 ammonium persulphate solution (APS) and finally set by the addition of 1.4 µl/ml TEMED
595 (NNN'N'-tetramethylethylenediamine). The stacking gel was then prepared again by adding the
596 appropriate amount of acrylamide to the stacking buffer (consisting of 0.1% w/v SDS, 125 mM
597 Tris). Polymerization was activated by adding 0.1% (v/v) APS and set using 4 µl/ml TEMED.
598 SDS-PAGE gels were run in a tank containing an electrode buffer (25 mM Tris, 0.1%
599 (v/v) glycerol, 190 mM glycine, diluted 1:10 with dH2O) at 90 V for approximately 90 min. 6 µl
600 PageRuler™ Plus Prestained Protein Ladder, 10 to 250 kDa (ThermoFisher Scientific) was
601 loaded as a protein size marker, displaying coloured bands at 10, 15, 25, 35, 55 70, 100, 130 and
602 250 kDa.
603
604 **Western Blotting**
605 Following electrophoresis, the SDS gels were first washed in 1x transfer buffer (0.04% (w/v)
606 SDS, 20% (v/v) methanol, 38 mM glycine, 48 mM Tris) for 5 minutes. The proteins were then
607 transferred overnight onto nitrocellulose membranes (Whatman, GE Healthcare Life Sciences,
608 Buckinghamshire, UK) in a 1 litre tank containing transfer buffer at 30 V.
609 The nitrocellulose membranes were incubated in milk buffer (5% (w/v) dried skimmed
610 milk powder (Tesco, Durham, UK), 150 mM NaCl, 10 mM Tris, 0.1% (v/v) Tween 20, pH 7.4)
611 for 20 min to block non-specific protein binding. Following this treatment, the membranes were
612 incubated with primary antibody for 2.5 h (GFP, Abcam, Cambridge, UK: rabbit, 1:10000; HA
613 (Roche), rat, 1:3000; Rubisco large subunit (Agrisera), rabbit, 1:10000). Excess primary antibody
614 was then removed by washing three times in 2x TBST (150 mM NaCl, 10 mM Tris, 0.1% (v/v)
615 Tween 20, pH 7.4) for 2 m, 5 min and 10 min, and subsequently incubated for 1 h with the ECL
616 peroxidase-labelled anti-rabbit or anti-rat IgG secondary antibody, diluted 1:20000 in TBST.
617 Excess secondary antibody was removed again by washing three times in 1x TBST, as with the
618 primary antibody. In order to visualize the probed blot, the membrane was incubated with ECL
619 Western Blotting Detection Reagent immediately prior to imaging. The horseradish peroxidase

620 conjugated to the secondary antibody was detected by using X-ray film, which was subsequently
621 developed in a dark room.
622
623 **Estimation of synthetic PLS concentration**
624 Freeze-dried synthetic PLS peptide (Cambridge Research Biochemicals, Billingham) was
625 dissolved in DMSO. An aliquot was added to aqueous buffer (10 mM HEPES pH7, 20 mM NaCl,
626 80 mM KCl) and absorbance at 280 nm was recorded. Concentration was estimated from the
627 absorbance and the ProtParam estimated extinction coefficient of 2,980 M^{-1} cm^{-1}. Concurrent
628 with this a sample was submitted for quantitative amino acid analysis (Abingdon Health
629 Laboratory Services). From this analysis a conversion factor of 2.27 was generated, which was
630 applied to concentrations determined by A280 nm.
631
632 **ATX1 purification**
633 *E. coli* BL21(DE3) containing pETatx1 was used to overexpress the wildtype *ATX1* gene from
634 *Arabidopsis thaliana* (optimised for expression in *E. coli*, Novoprolabs). Harvested cells were
635 collected and frozen at -20 ºC overnight then defrosted, resuspended in 20 mM HEPES (pH 7.0),
636 10 mM EDTA, 100 mM NaCl, 10 mM DTT. Cells were sonicated (Bandelin Sonoplus),
637 supernatant separated by size exclusion chromatography (GE Healthcare, HiLoad 26.600
638 Superdex 75 pg) metal-free buffer lacking EDTA. Fractions containing ATX1 were incubated
639 overnight and pooled before transfer into an anaerobic chamber (Belle Technology) via desalting
640 column where reductant was removed. ATX1 was quantified by combination of Bradford assay
641 and Ellman's reagent to ensure the fully reduced state of the protein. Samples were also analysed
642 for metal content by ICP-MS to ensure > 95% apo-ATX1.
643
644 **MBP-PLS/mutant purification**
645 A fusion of PLS to MBP was created using the NEBExpress MBP Fusion and Purification
646 System. Two complementary oligonucleotide primers encoding PLS (optimised for expression
647 in *E. coli*) were annealed and inserted into the pMal-c5x plasmid at XmnI and SalI insertion sites.
648 The three mutants MBP-PLS(C6S), MBP-PLS(C17S) and MBP-PLS(C6S/C17S) were
649 created by site-directed mutagenesis (QuikChange II, Agilent). *E. coli* NEB Express containing
650 the pMal plasmid with the correct MBP-PLS mutant was used to overexpress each protein.
651 Harvested cells were resuspended in 20 mM Tris-HCl (pH 7.4), 200 mM NaCl, 1 mM EDTA
652 and frozen at -20 ºC overnight. Cells were defrosted in cold H_2O, sonicated, purified by
653 ammonium sulphate precipitation (where MBP-PLS precipitates >60% saturation), separated on
654 MBP-trap (GE Healthcare) and eluted using buffer containing 10 mM maltose. MBP-PLS-
655 containing fractions were pooled and concentrated using centrifugal concentrator (Corning, Spin-
656 X UF 30 KDa) and buffer exchanged by desalting column into metal-free 20 mM HEPES (pH
657 7.0), 50 mM NaCl buffer in an anaerobic chamber (Belle Technology). Mutants containing thiols
658 were quantified Ellman's assay and MBP-PLS(C6S/C17S), which lacks all thiols, was quantified
659 by Bradford assay alone. Samples were also analysed for metal content by ICP-MS to ensure
660 >95% apo-protein.
661
662 **Anaerobic spectroscopic analysis of Cu(I) complexes**
663 All Cu(I) titration experiments were carried out in an anaerobic chamber (Belle Technology)
664 using metal-free CHELEX-treated, degassed buffers. For experiments titrating Cu(I), aqueous
665 $CuSO_4$ stock was quantified in advance by ICP-MS and diluted to working concentrations. The
666 reductant NH_2OH was included at final concentration of 1 mM to retain Cu(I) in its reduced state.
667 Proteins were diluted in buffer to the final concentration specified in each titration in air-tight

quartz cuvettes (Helma), and after addition of probe to the concentration specified, titrated with $CuSO_4$. After each addition, solutions were thoroughly mixed and absorbance spectra recorded using a Lambda 35 UV/Vis spectrophotometer (Perkin Elmer). Titration isotherm data was fitted using simulated affinity curves using DynaFit (*58*).

Interaction studies of PLS with copper transporter ETR1 by Microscale Thermophoresis

Fluorescently labelled ETR1 truncation mutants were added to a dilution series of PLS in 50 mM HEPES, 150 mM NaCl, 0.015 % (wv) FosCholine 16 (pH 7.6) or 50 mM Tris, 300 mM NaCl, 0.015 % (w/v) FosCholine 16 (pH 7.6). Dissociation constants were calculated using GraphPad Prism 5.

Determination of dissociation constants for the PLS-ETR1 interaction

Full-length ETR1 and truncation mutants were purified and labelled as described in (*59*). 94 µM PLS were diluted serially in 50 mM Tris and 300 mM NaCl (pH 7.6). Fluorescently labelled receptor was added at a final concentration of 50 nM. Thermophoretic behaviour was measured in premium capillaries at 50 % LED and 50 % MST power. In case of a binding event, data were fitted using GraphPad Prism 5.

Interaction studies of PLS with copper transporter RAN1 and copper chaperones by microscale thermophoresis

PLS was titrated to fluorescently labelled RAN1 and RAN1 truncation mutants. RAN1, NterRAN1 and CterRAN1 were purified and labelled as described in (*18*). NterRAN1 is a truncation containing only of two N-terminal metal-binding-domains, whereas CterRAN1 is a construct lacking this region. Direct interaction between PLS and RAN1 was observed using Microscale Thermophoresis. Dissociation constants indicate that PLS interacts predominantly with the N-terminal metal-binding-domains, but only weakly with the C-terminal region. Dissociation constants were determined using GraphPad Prism 5. Titration experiments were also carried out with fluorescently labelled copper chaperones ATX, CCH and CCHΔ, a mutant lacking the plant specific C-terminal extension. Proteins were purified and labelled as described (*18*).

Ratiometric analysis of roGFP2 fusion proteins

N- and C-terminal roGFP2 fusion proteins of PLS were generated by Gateway cloning. Infiltration and transient expression of roGFP2 fusions and control proteins were carried out as described (*26*). Image acquisition and data analysis were carried out as described in (*18*). A minimum of 10 leaf optical sections were imaged and used for ratiometric analysis of the redox sensitive excitation properties of roGFP2.

Statistical methods

For gene expression analysis and growth assays, a minimum of three biological replicates was used - see Supplementary Materials, Figure legends, Supplementary Tables (*20*). For protein-protein interaction and protein localization studies, assays were carried out independently between 2 and 10 times (Figs. 2, 3 legends). At least three biological replicates were used for plant growth assays, RNA-seq and gene expression (RT-qPCR) experiments, metal binding assays (Fig. 4). Normalised values from at least three biological replicates were then used for one- or two-way analysis of variance (ANOVA) where appropriate and indicated in relevant Figure legends. Error bars are defined in Figure legends, where relevant.

Data Availability.

All study data are included in the article and/or Supplementary Information. RNA-seq and root assay data are available at GEO accession GSE256166: https://eur01.safelinks.protection.outlook.com/?url=https%3A%2F%2Fwww.ncbi.nlm.nih.gov%2Fgeo%2Fquery%2Facc.cgi%3Facc%3DGSE256166&data=05%7C02%7Ckeith.lindsey%40durham.ac.uk%7C9637f7022a2240cfb10608dc324244cd%7C7250d88b4b684529be44d59a2d8a6f94%7C0%7C0%7C638440507397042151%7CUnknown%7CTWFpbGZsb3d8eyJWIjoiMC4wLjAwMDAiLCJQIjoiV2luMzIiLCJBTiI6Ik1haWwiLCJXVCI6Mn0%3D%7C0%7C%7C%7C%7C&sdata=U4JHCoviYbdEbF76Tws8Ridq7W%2B5Hq2qBVN%2BFjIysgw%3D&reserved=0

References

1. Johnson, P.R., Ecker J.R. The ethylene gas signal transduction pathway: A molecular perspective. *Ann. Rev. Genet.* ***32***, 227-254 (1998).

2. Chang, C., Kwok, S.F., Bleecker, A.B., Meyerowitz, E.M. Arabidopsis ethylene-response gene *ETR1* - similarity of product to 2-component regulators. *Science* **262**, 539-544 (1993).

3. Hua, J., Chang, C., Sun, Q., Meyerowitz, E.M. Ethylene insensitivity conferred by Arabidopsis *ERS* gene. *Science* **269**, 1712-1714 (1995).

4. Hua, J., Sakai, H., Nourizadeh, S., Chen, Q.G., Bleecker, A.B., Ecker, J.R., Meyerowitz, E.M. EIN4 and ERS2 are members of the putative ethylene receptor gene family in Arabidopsis. *Plant Cell* **10**, 1321-1332 (1998).

5. Sakai, H., Hua, J., Chen, Q.G., Chang, C., Medrano, L.J., Bleecker, A.B., Meyerowitz, E.M. *ETR2* is an *ETR1*-like gene involved in ethylene signaling in *Arabidopsis*. *Proc. Natl. Acad. Sci. USA* **95**, 5812-5817 (1998).

6. Chen, Y.F., Randlett, M.D., Findell, J.L., Schaller, G.E. Localization of the ethylene receptor ETR1 to the endoplasmic reticulum of Arabidopsis. *J. Biol. Chem*. **277**, 19861-19866 (2002).

7. Grefen, C., Staedele, K., Ruzicka, K., Obrdlik, P., Harter, K., Horak, J. Subcellular localization and in vivo interactions of the *Arabidopsis thaliana* ethylene receptor family members. *Molec. Plant* **1**, 308-320 (2008).

8. Schaller, G.E., Ladd, A.N., Lanahan, M.B., Spanbauer, J.M., Bleecker, A.B. The ethylene response mediator ETR1 from Arabidopsis forms a disulfide-linked dimer. *J. Biol. Chem*. **270**, 12526-12530 (1995).

9. Hall, A.E., Findell, J.L., Schaller, G.E., Sisler, E.C., Bleecker, A.B. Ethylene perception by the ERS1 protein in Arabidopsis. *Plant Physiol.* **123**, 1449-1457 (2000).

10. Rodriguez, F.I., Esch, J.J., Hall, A.E., Binder, B.M., Schaller, G.E., Bleecker, A.B. A copper cofactor for the ethylene receptor ETR1 from Arabidopsis. *Science* **283**, 996-998 (1999).

11. McDaniel, B.K., Binder, B.M. ETHYLENE RECEPTOR 1 (ETR1) is sufficient and has the predominant role in mediating inhibition of ethylene responses by silver in *Arabidopsis thaliana*. *J. Biol. Chem.* **287**, 26094-26103 (2012).

12. Chang, C.R. Ethylene signaling: the MAPK module has finally landed. *Trends Plant Sci.* **8**, 365-368 (2003).

13. Gao, Z.Y., Chen, Y.-F., Randlett, M.D., Zhao, X.-C., Findell, J.L., Kieber, J.J., Schaller, G.E. Localization of the Raf-like kinase CTR1 to the endoplasmic reticulum of Arabidopsis through participation in ethylene receptor signaling complexes. *J. Biol. Chem*. **278**, 34725-34732 (2003).

14. Chilley, P.M., Casson, S.A., Tarkowski, P., Hawkins, N., Wang, K.L., Hussey, P.J., Beale, M., Ecker, J.R., Sandberg, G.K., Lindsey, K. The POLARIS peptide of Arabidopsis regulates auxin transport and root growth via effects on ethylene signaling. *Plant Cell* **18**, 3058-3072 (2006).

15. Hirayama, T., Kieber, J.J., Hirayama, N., Kogan, M., Guzman, P., Nourizadek, S., Alonso, J.M., Dailey, W.P., Dancis, A., Ecker, J.R. RESPONSIVE-TO-ANTAGONIST1, a Menkes/Wilson disease-related copper transporter, is required for ethylene signaling in Arabidopsis. *Cell* **97**, 383-393 (1999).

16. Binder, B.M., Rodriguez, F.I., Bleecker, A.B. The copper transporter RAN1 is essential for biogenesis of ethylene receptors in Arabidopsis. *J. Biol. Chem*. **285**, 37263-37270 (2010).

17. Qu, X., Hall, B.P., Gao, Z.Y., Schaller, G.E. A strong constitutive ethylene-response phenotype conferred on Arabidopsis plants containing null mutations in the ethylene receptors *ETR1* and *ERS1*. *BMC Plant Biol*. **7**, 3 (2007).

18. Hoppen, C., Müller, L., Hänsch, S., Uzun, B., Milic, D., Meyer, A.J., Weidtkamp-Peters, S., Groth, G. Soluble and membrane-bound protein carrier mediate direct copper transport to the ethylene receptor family. *Sci Rep.* **9**, 10715 (2019).

19. Casson, S.A., Chilley, P.M., Topping, J.F., Evans, I.M., Souter, M.A., Lindsey, K. The *POLARIS* gene of Arabidopsis encodes a predicted peptide required for correct root growth and leaf vascular patterning. *Plant Cell* **14**, 1705-1721 (2002).

20. Mudge, A.J., Mehdi, S., Michaels, W., Orosa-Puente, B., Shen, W., Wei, W., Tomlinson, C., Sadanandom, A., Hetherington, F.M., Hoppen, C., Uzun, B., Groth, G., Topping, J.F., Robinson, N.J., Lindsey, K. Data from: A peptide that regulates metalation and function of the *Arabidopsis* ethylene receptor. GEO accession GSE256166: https://eur01.safelinks.protection.outlook.com/?url=https%3A%2F%2Fwww.ncbi.nlm.nih.gov%2Fgeo%2Fquery%2Facc.cgi%3Facc%3DGSE256166&data=05%7C02%7Ckeith.lindsey%40durham.ac.uk%7C9637f7022a2240cfb10608dc324244cd%7C7250d88b4b684529be44d59a2d8a6f94%7C0%7C0%7C638440507397042151%7CUnknown%7CTWFpbGZsb3d8eyJWIjoiMC4wLjAwMDAiLCJQIjoiV2luMzIiLCJBTiI6Ik1haWwiLCJXVCI6Mn0%3D%7C0%7C%7C%7C&sdata=U4JHCoviYbdEbF76Tws8Ridq7W%2B5Hq2qBVN%2BFjIysgw%3D&reserved=0

811 21. Liu, J., Mehdi, S., Topping, J., Tarkowski, P., Lindsey, K. Modelling and experimental
812 analysis of hormonal crosstalk in Arabidopsis. *Molec. Systems Biol*. **6**, 373 (2010).
813
814 22. Liu, J.L., Mehdi, S., Topping, J., Friml, J., Lindsey, K. Interaction of PLS and PIN and
815 hormonal crosstalk in Arabidopsis root development. *Front. Plant Sci.* **4**, 75 (2013).
816
817 23. Moore, S., Zhang, X., Mudge, A., Rowe, J.H., Topping, J.F., Liu, J., Lindsey, K.
818 Spatiotemporal modelling of hormonal crosstalk explains the level and patterning of hormones
819 and gene expression in *Arabidopsis thaliana* wildtype and mutant roots. *New Phytol*. **207**, 1110-
820 1122 (2015).
821
822 24. Lee, H., Sparkes, I., Gattolin, S., Dzimitrowicz, N., Roberts, L.M., Hawes, C., Frigerio, L.
823 An Arabidopsis reticulon and the atlastin homologue *RHD3-like2* act together in shaping the
824 tubular endoplasmic reticulum. *New Phytol.* **197**, 481-489 (2013).
825
826 25. Bauer, M., Papenbrock, J. Identification and characterization of single-domain thiosulfate
827 sulfurtransferases from Arabidopsis thaliana. *FEBS Lett*. **532**, 427-431 (2002).
828
829 26. Brach, T., Soyk, S., Müller, C., Hinz, G., Hell, R., Brandizzi, F., Meyer, A.J. Non-invasive
830 topology of membrane proteins in the secretory pathway. *Plant J.* **57**, 534-541 (2009).
831
832 27. Schott-Verdugo, S., Müller, L., Classen, E., Gohlke, H., Groth, G. Structural model of the
833 ETR1 ethylene receptor transmembrane sensor domain. *Sci Rep.* **9,** 8869 (2019).
834
835 28. Robinson, N.J., Winge, D.R. Copper metallochaperones. *Ann. Rev. Biochem.* **79**, 537-562
836 (2010).
837
838 29. Xiao, Z., Brose, J., Schimo, S., Ackland, S.M., La Fontaine, S., Wedd, A.G. Unification of
839 the copper(I) binding affinities of the metallo-chaperones Atx1, Atox1, and related proteins:
840 detection probes and affinity standards. *J. Biol. Chem.* **286**, 11047-11055 (2011).
841
842 30. Morgan, M.T., Bourassa, D., Harankhedkar, S., McCallum, A.M., Zlatic, S.A., Calvo, J.S.,
843 Meloni, G., Faundez, V., Fahrni, C.J. Ratiometric two-photon microscopy reveals attomolar
844 copper buffering in normal and Menkes mutant cells. *Proc. Natl. Acad. Sci. USA* **116**, 12167–
845 12172 (2019).
846
847 31. Yu, C.H., Yang, N., Bothe, J., Tonelli, M., Nokhrin, S., Dolgova, N. V., Braiterman, L.,
848 Lutsenko, S., Dmitriev, O.Y. The metal chaperone Atox1 regulates the activity of the human
849 copper transporter ATP7B by modulating domain dynamics. *J. Biol. Chem.* **292**, 18169 (2017).
850
851 32. Li, W., Lacey, R.F., Ye, Y., Lu, J., Yeh, K.-C., Xiao, Y., Li, L., Wen, C.-K., Binder, B.M.,
852 Zhao, Y. Triplin, a small molecule, reveals copper ion transport in ethylene signaling from ATX1
853 to RAN1. *PLOS Genet.* **13**, e1006703.
854
855 33. Campos, M. L., de Souza, C. M., de Oliviera, K.B.S., Dias, S.C., Franco, O.L. The role of
856 antimicrobial peptides in plant immunity. *J. Exp. Bot.* **69**, 4997-5011 (2018).
857
858 34. Willoughby, A.C., Nimchuk , Z.L. WOX going on: CLE peptides in plant development. *Curr.*

859 *Opin. Plant Biol.* **63**, 102056 (2021).
860
861 35. Kim, J.S., Jeon, B.W., Kim, J. Signaling peptides regulating abiotic stresses in plants. *Front.*
862 *Plant Sci.* **12**, 704490 (2021).
863
864 36. Olsson, V., Joos, L., Zhu, S., Gevaert, K., Butenko, M., De Smet, I. Look closely, the
865 beautiful may be small: Precursor-derived peptides in plants. *Ann. Rev. Plant Biol.* **70**, 153-186
866 (2019).
867
868 37. Duckert, P., Brunak, S., Blom, N. Prediction of preprotein convertase cleavage sites. *Prot.*
869 *Engin. Design Select.* **17**, 107-112 (2004).
870
871 38. Capraro, J., Sessa, F., Magni, C., Scarafoni, A., Maffioloi, E., Tedeschi, G., Croy, R.D.D,
872 Duranti, M. Proteolytic cleavage at twin arginine residues affects structural and functional
873 transitions of Lupin seed 11S storage globulin. *PLOS ONE* **10**, e0117406.

874 39. Casareno RL, Waggoner D, Gitlin JD (1998) The copper chaperone CCS directly interacts
875 with copper/zinc superoxide dismutase. J Biol Chem 273: 23625–23628

876 40. Chu, C.C., Lee, W.C., Guo, W.Y., Pan, S.M., Chen, L.J., Li , H.M., Jinn, T.L. A copper
877 chaperone for superoxide dismutase that confers three types of copper/zinc superoxide
878 dismutase activity in Arabidopsis. *Plant Physiol*. **139**, 425–436 (2005).

879 41. Puig, S., Mira, H., Dorcey, E., Sancenón, V., Andrés-Colás, N., Garcia-Molina, A., Burkhead,
880 J.L., Gogolin, K.A., Abdel-Ghany, S.E., Thiele, D.J., Ecker, J.R., Pilon, M., Penarrubia, L.
881 Higher plants possess two different types of ATX1-like copper chaperones. *Biochem. Biophys.*
882 *Res. Commun*. **354**, 385–390 (2007).

883 42. Andrés-Colás, N., Sancenón, V., Rodríguez-Navarro, S., Mayo, S., Thiele, D.J., Ecker,
884 J.R., Puig, S., Peñarrubia, L. The Arabidopsis heavy metal P-type ATPase HMA5 interacts
885 with metallochaperones and functions in copper detoxification of roots. *Plant J*. **45**, 225–236
886 (2006).

887 43. Williams, L.E., Mills, R.F. P (1B)-ATPases: an ancient family of transition metal pumps
888 with diverse functions in plants. *Trends Plant Sci.* **10**, 491–502 (2005).

889 44. Burkhead, J.L., Reynolds, K.A., Abdel-Ghany, S.E., Cohu, C.M., Pilon, M. Copper
890 homeostasis. *New Phytol.* **182**, 799–816 (2009).

891 45. Shin, L.-J., Lo, J.-C., Yeh, K.-C. Copper chaperone antioxidant protein1 is essential for
892 copper homeostasis. *Plant Physiol.* **159**, 1099-1110 (2012).
893
894 46. Sabatini, S., Beis, D., Wolkenfelt, H., Murfett, J., Guilfoyle, T., Malamy, J., Benfey, P.,
895 Leyser, O., Bechtold, N., Weisbeek, P., and Scheres, B. An auxin- dependent distal organizer of
896 pattern and polarity in the Arabidopsis root. *Cell* **99,** 463-472 (1999).
897

47. Abel, S., Nguyen, M., Chow, W. and Theologis, A. *ASC4*, a primary indoleacetic acid-responsive gene encoding 1-amino-cyclopropane-1-carboxylate synthase in *Arabidopsis thaliana*. *J. Biol. Chem*. **270**, 19093–19099 (1995).

48. Ortega-Martinez, O., Pernas, M., Carol, R.J., and Dolan, L. Ethylene modulates stem cell division in the Arabidopsis thaliana root. *Science* **317**, 507- 510 (2007).

49. Matsuzaki, Y., Ogawa-Ohnishi, M., Mori, A., Matsubayashi, Y. Secreted peptide signals required for maintenance of root stem cell niche in Arabidopsis. *Science* **329**, 1065-1067 (2010).

50. Clough, S.J., Bent, A.F. Floral dip: a simplified method for *Agrobacterium*-mediated transformation of *Arabidopsis thaliana*. *Plant J*. **6**, 735-743 (1998).

51. Thompson, H.L., Shen, W., Matus, R., Kakkar, M., Jones, C., Dolan, D., Grellscheid, S., Yang, X., Zhang, N., Mozaffari-Jovin, S., Chen, C., Zhang, X., Topping, J.F., Lindsey, K. MERISTEM-DEFECTIVE regulates the balance between stemness and differentiation in the root meristem through RNA splicing control. *Development* **150**, dev201476.

52. Dobin, A., Davis, C.A., Schlesinger, F., Drenkow, J., Zaleski, C., Jha, S., Batut, P.,; Chaisson, M., Gingeras, T.R. STAR: ultrafast universal RNA-seq aligner. *Bioinformatics*, **29**, 15-21 (2013).

53. Love, M.I., Huber, W., Anders, S. Moderated estimation of fold change and dispersion for RNA-seq data with DESeq2. *Genome Biol.* **15**, 550 (2014).

54. Tian, T., Liu, Y., Yan, H., You, Q., Yi, X., Du, Z., Xu, W., Su, Z. agriGO v2.0: a GO analysis toolkit from the agricultural community, 2017 update. *Nicl. Acids Res.* **45**, W122-W129 (2017).

55. Zhong, S., Lin, Z., Grierson, D. Tomato ethylene receptor-CTR interactions: visualization of NEVER-RIPE interactions with multiple CTRs at the endoplasmic reticulum. *J. Exp. Bot.* **59**, 965-972 (2008).

56. Brandizzi, F., Snapp, E.L., Roberts, A.G., Lippincott-Schwartz, J., Hawes, C. Membrane protein transport between the endoplasmic reticulum and the golgi in tobacco leaves is energy dependent but cytoskeleton independent: Evidence from selective photobleaching. *Plant Cell* **14**, 1293-1309 (2002).

57. Voinnet, O., Rivas, S., Mestre, P., Baulcombe, D. An enhanced transient expression system in plants based on suppression of gene silencing by the p19 protein of tomato bushy stunt virus. *Plant J*. **33**, 949-956 (2003).

58. Kuzmič, P. DynaFit—A Software Package for Enzymology. *Meth. Enzymol*. **467**, 247–280 (2009).

59. Milić, D., Dick, M., Mulnaes, D., Pfleger, C., Kinnen, A., Gohlke, H. *et al.*, Recognition motif and mechanism of ripening inhibitory peptides in plant hormone receptor ETR1. *Sci. Rep.* **8**, 1–12 (2018).

Acknowledgements: We thank Prof. Steven Cobb (Durham University Department of Chemistry) for advice on peptide synthesis, and Dr. Andrew Foster (Durham University Department of Chemistry) for preliminary peptide-Cu interaction analysis. The authors acknowledge financial support from: UK Biotechnology and Biological Sciences Research Council BB/E006531/1, BBS/B/0773X, BB/J014516/1 (KL), BB/V006002/1, BB/M011186/1 (NJR); Deutsche Forschungsgemeinschaft (German Research Foundation) 267205415 – SFB 1208 project B06 (GG).

Author contributions:
KL and NJR initiated the project. KL, JFT, NJR, AS and GG designed and supervised aspects of the project. AJM, SM, WM, BO-P, WS, WW, CT, DR, FMH, CH and BU carried out the experimental work and prepared the Figures. KL, NJR and GG drafted the early version of the manuscript, and all authors reviewed and edited the manuscript.

Competing interests: Authors declare no competing interests.

963 **Figure Legends**
964
965 **Figure 1. The PLS peptide is required for ethylene control of seedling growth, is**
966 **structurally and functionally conserved, and complements the *Arabidopsis pls* mutant.**
967 (**a**). Amino acid sequence of the PLS peptide from *Arabidopsis thaliana* with *Camelina sativa*
968 PLS sequence (*C.s*), and synthetic truncations N1, N2, C1 and C2, indicated by horizontal lines.
969 Two cysteine residues are highlighted in bold. (**b**) Wildtype (left) and *pls* mutant (right); bar = 5
970 mm. (**c**) Expression levels of 24 ethylene-responsive genes in *pls* and *PLS* overexpressing
971 (PLSox) seedlings, compared to wildtype levels. Data are expressed as $\log_2$-fold changes in *pls*
972 mutant and PLSox seedlings compared wildtype with respective significance levels (*P-adj* value)
973 provided in Table S1. A $P < 0.05$ and $\log_2$-fold of change of ± 0.5 was chosen to identify
974 differentially expressed genes. (**d**) Effect of *Arabidopsis* PLS full length peptide, *A.t.* PLS(FL),
975 and *Camelina* PLS peptide (*C.s.* PLS) on *Arabidopsis* primary root length. Wildtype (C24; blue
976 bars) and *pls* mutant seedlings (red bars) were grown hydroponically in the presence (100 nM)
977 or absence of peptide for 10 d. (**e**) Effect of PLS full length and truncated peptides on wild type
978 (blue bars) and *pls* mutant (red bars) *Arabidopsis* primary root length. Seedlings were grown
979 hydroponically in the presence of 50 nM peptide for 10 d. C1 = C-terminal 14 amino acids, C2
980 = C-terminal 24 amino acids, N1 = N-terminal 22 amino acids, N2 = N-terminal 9 amino acids,
981 full length PLS = 36 amino acids. Error bars show ± 1 standard error, n = 25.
982
983 **Figure 2. PLS localizes to the endoplasmic reticulum.**
984 (**a-o**) PLS::PLS:GFP fusion protein (**a, g, j**) colocalizes with endoplasmic reticulum markers ER
985 Tracker (**b, c, c inset**) and RFP:HDEL (**h, i, i inset**), but free GFP does not (**d-f**, **m-o**). PLS:GFP
986 staining is seen also in nuclei (n). PLS::PLS:GFP (**j**) does not co-localize with the *trans*-Golgi
987 markers ST-mCherry SH:GFP (**k, l**). Scale bars = 25 µm (**c, l**), 10 µm (**f, i, o**). Root epidermal
988 cells in the transition zone were imaged. (**p**) Ratiometric analysis of roGFP2 fusion constructs
989 transiently expressed in *N. benthamiana*. Comparison of excitation ratios of PLS-roGFP2 and
990 roGFP2-PLS with control constructs (free roGFP, SEC22 fusions) reveals that PLS localizes to
991 the cytosolic side of the ER.
992
993 **Figure 3. PLS interacts with the ethylene receptor ETR1.**
994 (**a**) Co-immunoprecipitation of PLS:GFP by ETR1:HA (upper panel) in leaves of *Nicotiana*
995 *benthamiana*, in the presence and absence of 0.5 µM $CuSO_4$ and EDTA (to remove Cu). Lower
996 panels show presence of ETR1:HA in extracts using anti-HA antibody, and protein input blots
997 using anti-GFP and anti-Rubisco. (**b**) Densitometric scan of immunoblot. (**c**) Competition assay
998 showing a reduced binding between PLS:GFP and ETR1:HA in the presence of 0, 5 nM or 25
999 nM PLS peptide, in the presence of 0.5 µM $CuSO_4$ and 50 µM MG-132, a proteasome inhibitor
1000 (upper panel). Lower panel shows ETR1:HA in extracts using anti-HA antibody. (**d**)
1001 Densitometric scan of immunoblot. (**e**) Co-immunopreciptation of ETR1:HA (upper panel) in
1002 leaves of *N. benthamiana*, showing the effect of EDTA (to remove Cu) on interaction between
1003 ERT1:HA and PLS:GFP. Lower panels shows presence of ETR1:HA in extracts using anti-HA
1004 antibody, and protein input blots using anti-ETR1-HA and anti-Rubisco. (**f**) Densitometric scan
1005 of immunoblot. α-GFP, anti-GFP antibody; α-HA, anti-HA antibody. (**g**) Microscale
1006 thermophoresis binding curves of different ETR1 truncations with PLS. Binding of PLS was
1007 observed with full-length ETR1 and all C-terminal truncations but not with $ETR1^{306-738}$ lacking
1008 the N-terminal transmembrane part of the receptor.
1009
1010

1011 **Figure 4. PLS binds copper and interacts with RAN1 and copper chaperones.**
1012 (**a**) C6S and C17S in PLS are required for function. Seedlings were grown hydroponically for 10
1013 d in the presence (100 nM) or absence of peptide (FL or C6S, C17S). Blue bars are C24, red bars
1014 are *pls*. Asterisk: ANOVA, F2, 51 = 9.48, p = 3.15E-4, Tukey's HSD. Error bars show ± 1
1015 standard error, n = 14-22. (**b**) BCA absorbance in the presence of synthetic PLS (19.8 μM, filled
1016 symbols) or an equivalent volume (to PLS) of DMSO (open symbols). Experiments with PLS
1017 used 88.3 μM (circles), 84 μM (triangles) and 88.4 μM (squares) BCA. The control experiment
1018 with DMSO used 85.3 μM BCA. (**c**) UV-vis apo subtracted difference spectra of synthetic PLS
1019 (19.8 μM) upon titration with CuCl (top left); binding isotherm of the feature at 242 nm (top
1020 right). Fluorescence spectra of PLS (19.8 μM) upon titration with CuCl (bottom left); binding
1021 isotherm of the feature at 306 nm (bottom right). (**d**) Absorption of BCA (17.3 μM) titrated with
1022 Cu(I) (representative spectrum, n = 2, full data in Fig. S6). (**e**) Binding isotherms ($A_{358\ nm}$) of
1023 BCA (10 μM) in the presence/absence (filled/empty symbols, respectively) of 14 μM MBP-PLS
1024 (circles) or MBP-PLS mutants (C6S, C17S and C6S/C17S: triangles, diamonds and squares
1025 respectively) titrated with Cu(I) (n = 3, ± SD). (**f**) Binding isotherms ($A_{358\ nm}$) of BCA (50 μM)
1026 in the presence/absence of 10 μM MBP-PLS (filled/empty symbols, respectively) titrated with
1027 Cu(I). Model (solid line) describes Cu(I)-binding as a 2:1 complex, with β_2 affinity of 3.79 (±
1028 1.5) $x10^{19}$ M^{-2}. Dotted lines simulate 10x weaker or tighter affinity (n = 3, ± SD). (**g**) Simulated
1029 Cu(I) occupancy (Supplementary Text) as a function of [PLS] using β_2 Cu(I) affinity of 3.79
1030 $x10^{19}$ M^{-2}. Inset, *Arabidopsis* ATX1 (20 μM, filled circles) withholds one Cu(I) equivalent from
1031 20 μM BCA (open circles, BCA-alone) (n = 3, ±SD), with K_D Cu(I) 5.47 $x10^{-18}$ M (Fig. S3). (**h**)
1032 Microscale thermophoresis binding curves of copper transporter RAN1 with PLS. (**i**) Microscale
1033 thermophoresis binding curves of soluble copper chaperones ATX1 and CCH with PLS (n = 3,
1034 ± SD).
1035
1036

a MKPRLCFNSRRRSISPCYISIS *C.s*

MKPRLCFNFRRRSISPCYISISYLLVAKLFKLFKIH

N2 N1 C1 C2

b

c

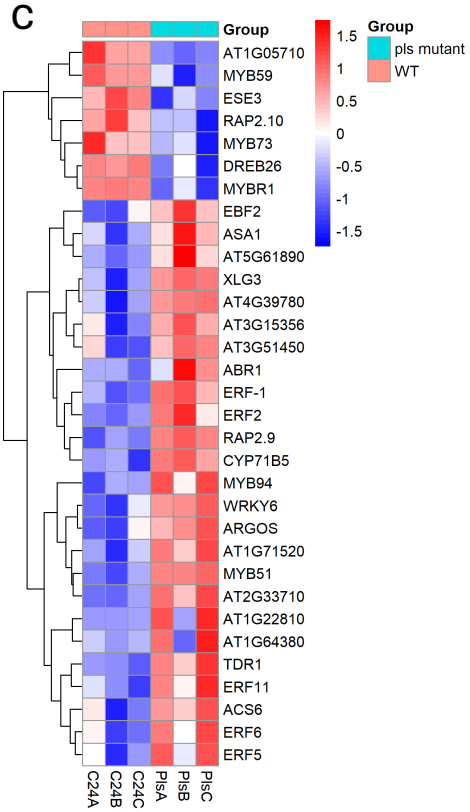

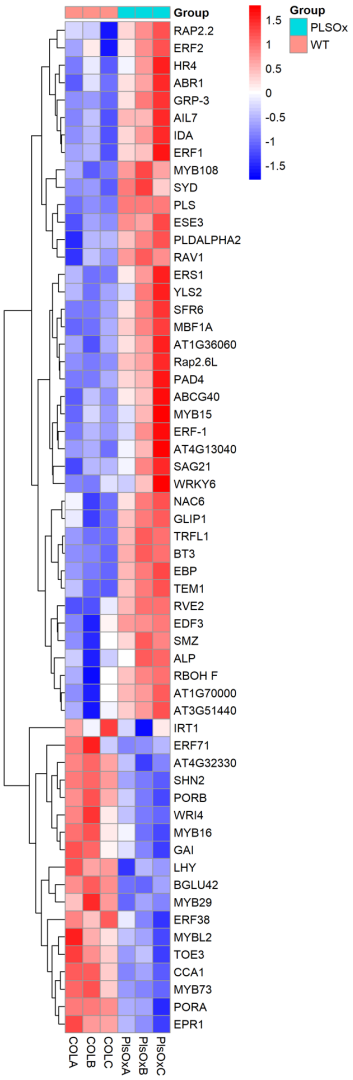

d

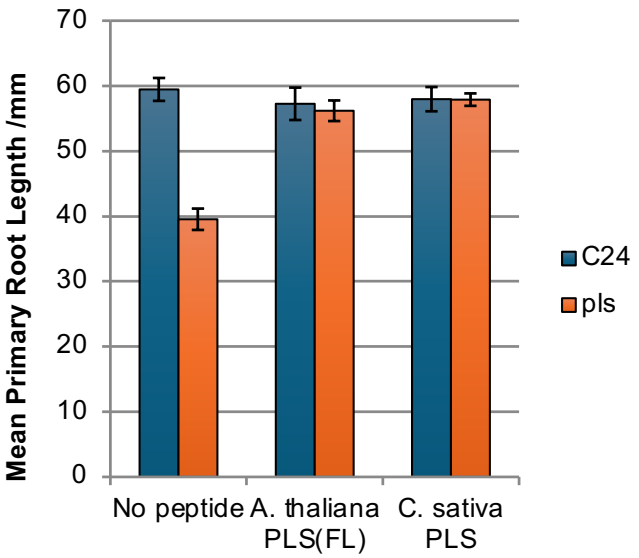

e

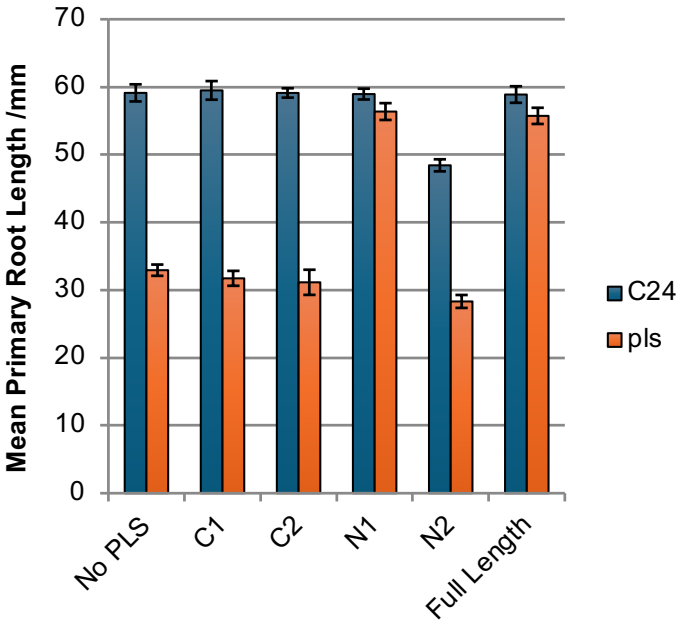

Fig. 1

Figure 1. The PLS peptide is required for ethylene control of seedling growth, is structurally and functionally conserved, and complements the *Arabidopsis pls* mutant.

(**a**). Amino acid sequence of the PLS peptide from *Arabidopsis thaliana* with *Camelina sativa* PLS sequence (*C.s*), and synthetic truncations N1, N2, C1 and C2, indicated by horizontal lines. Two cysteine residues are highlighted in bold. (**b**) Wildtype (left) and *pls* mutant (right); bar = 5 mm. (**c**) Heat maps showing expression levels of 32 ethylene-responsive genes in *pls* (left panel) and of 58 genes in *PLS* overexpressing (PLSox) seedlings (right panel), compared to wildtype levels. Data for 3 biological replicates are shown, and are expressed as $\log_2$-fold changes in *pls* mutant and PLSox seedlings compared wildtype with respective significance levels (*P-adj* value) provided in Tables S1 and S2. A $P < 0.05$ and $\log_2$-fold of change of $\pm$ 0.5 was chosen to identify differentially expressed genes. (**d**) Effect of *Arabidopsis* PLS full length peptide, *A.t.* PLS(FL), and *Camelina* PLS peptide (*C.s.* PLS) on *Arabidopsis* primary root length. Wildtype (C24; blue bars) and *pls* mutant seedlings (red bars) were grown hydroponically in the presence (100 nM) or absence of peptide for 10 d. (**e**) Effect of PLS full length and truncated peptides on wild type (blue bars) and *pls* mutant (red bars) *Arabidopsis* primary root length. Seedlings were grown hydroponically in the presence of 50 nM peptide for 10 d. C1 = C-terminal 14 amino acids, C2 = C-terminal 24 amino acids, N1 = N-terminal 22 amino acids, N2 = N-terminal 9 amino acids, full length PLS = 36 amino acids. Error bars show $\pm$ 1 standard error, n = 25.

Fig. 2

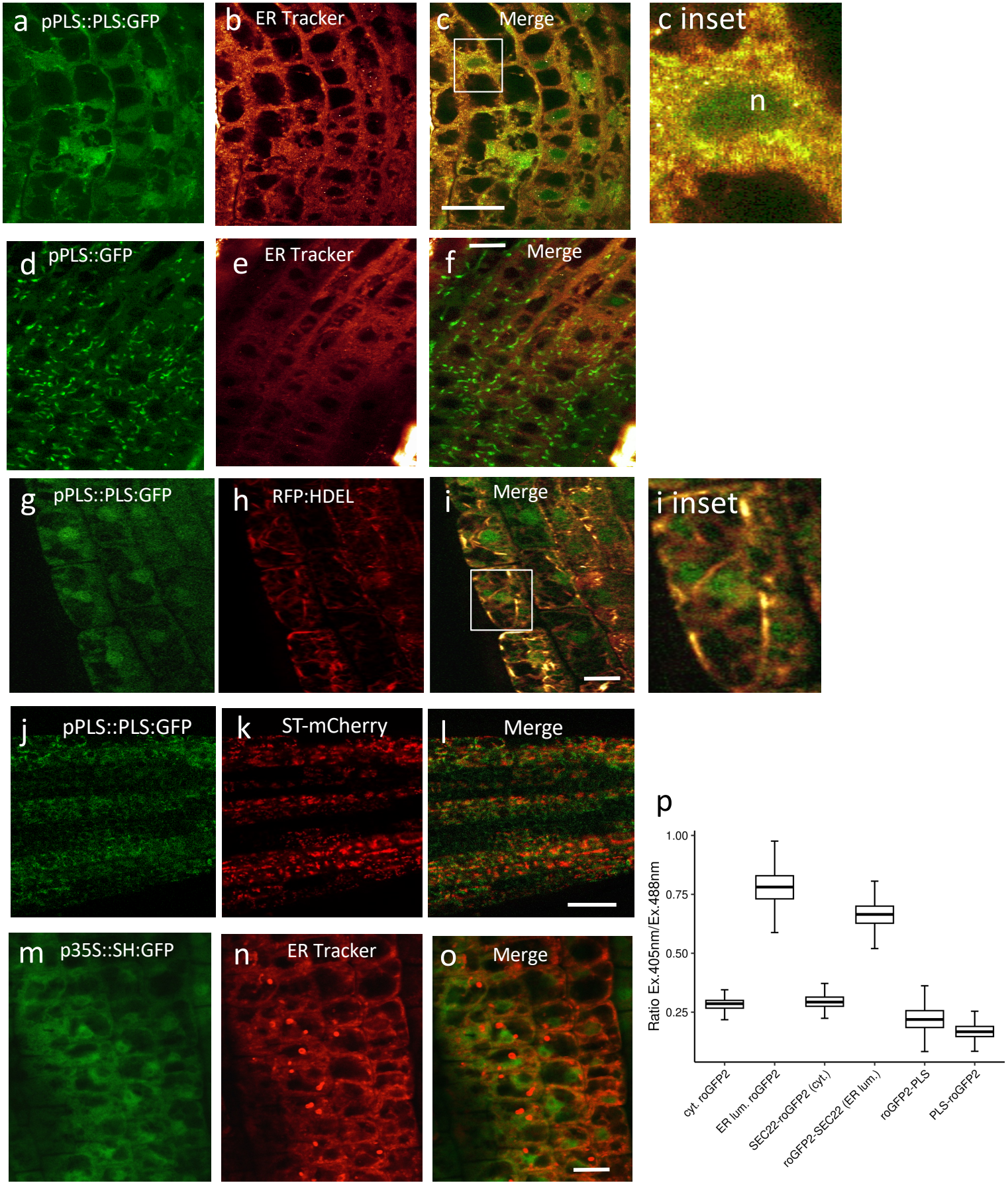
a pPLS::PLS:GFP
b ER Tracker
c Merge
c inset
n
d pPLS::GFP
e ER Tracker
f Merge
g pPLS::PLS:GFP
h RFP:HDEL
i Merge
i inset
j pPLS::PLS:GFP
k ST-mCherry
l Merge
m p35S::SH:GFP
n ER Tracker
o Merge
p
Ratio Ex.405nm/Ex.488nm
1.00
0.75
0.50
0.25
cyt. roGFP2
ER lum. roGFP2
SEC22-roGFP2 (cyt.)
roGFP2-SEC22 (ER lum.)
roGFP2-PLS
PLS-roGFP2

Figure 2. PLS localizes to the endoplasmic reticulum.
(**a-o**) PLS::PLS:GFP fusion protein (**a, g, j**) colocalizes with endoplasmic reticulum markers ER Tracker (**b, c, c inset**) and RFP:HDEL (**h, i, i inset**), but free GFP does not (**d-f**, **m-o**). PLS:GFP staining is seen also in nuclei (n). PLS::PLS:GFP (**j**) does not co-localize with the *trans*-Golgi markers ST-mCherry SH:GFP (**k, l**). Scale bars = 25 μm (**c, l**), 10 μm (**f, i, o**). Root epidermal cells in the transition zone were imaged. (**p**) Ratiometric analysis of roGFP2 fusion constructs transiently expressed in *N. benthamiana*. Comparison of excitation ratios of PLS-roGFP2 and roGFP2-PLS with control constructs (free roGFP, SEC22 fusions) reveals that PLS localizes to the cytosolic side of the ER.

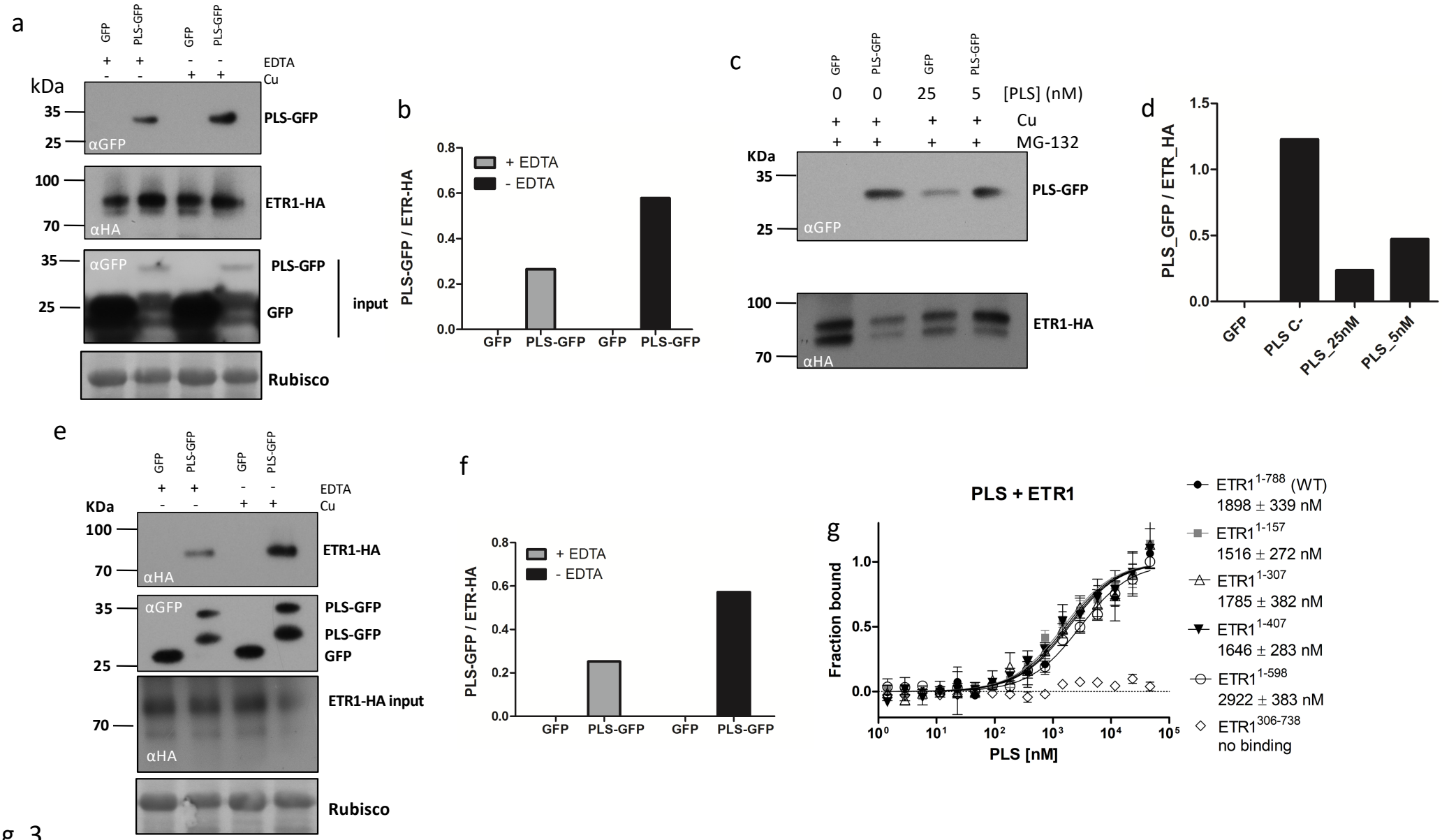
a
GFP
PLS-GFP
GFP
PLS-GFP
EDTA
Cu
kDa
35
25
αGFP
PLS-GFP
100
70
αHA
ETR1-HA
35
25
αGFP
PLS-GFP
GFP
input
Rubisco
b
PLS-GFP / ETR-HA
+ EDTA
- EDTA
0.8
0.6
0.4
0.2
0.0
GFP
PLS-GFP
GFP
PLS-GFP
c
GFP
PLS-GFP
GFP
PLS-GFP
0
0
25
5
[PLS] (nM)
Cu
MG-132
KDa
35
25
αGFP
PLS-GFP
100
70
αHA
ETR1-HA
d
PLS_GFP / ETR_HA
1.5
1.0
0.5
0.0
GFP
PLS C-
PLS_25nM
PLS_5nM
e
GFP
PLS-GFP
GFP
PLS-GFP
EDTA
Cu
KDa
100
70
αHA
ETR1-HA
35
25
αGFP
PLS-GFP
PLS-GFP
GFP
70
αHA
ETR1-HA input
Rubisco
f
PLS-GFP / ETR-HA
+ EDTA
- EDTA
0.8
0.6
0.4
0.2
0.0
GFP
PLS-GFP
GFP
PLS-GFP
g
PLS + ETR1
Fraction bound
1.0
0.5
0.0
10^0
10^1
10^2
10^3
10^4
10^5
PLS [nM]
ETR1$^{1-788}$ (WT)
1898 ± 339 nM
ETR1$^{1-157}$
1516 ± 272 nM
ETR1$^{1-307}$
1785 ± 382 nM
ETR1$^{1-407}$
1646 ± 283 nM
ETR1$^{1-598}$
2922 ± 383 nM
ETR1$^{306-738}$
no binding

Fig. 3

Figure 3. PLS interacts with the ethylene receptor ETR1.

(**a**) Co-immunoprecipitation of PLS:GFP by ETR1:HA (upper panel) in leaves of *Nicotiana benthamiana*, in the presence and absence of 0.5 μM $CuSO_4$ and EDTA (to remove Cu). Lower panels show presence of ETR1:HA in extracts using anti-HA antibody, and protein input blots using anti-GFP and anti-Rubisco. (**b**) Densitometric scan of immunoblot. (**c**) Competition assay showing a reduced binding between PLS:GFP and ETR1:HA in the presence of 0, 5 nM or 25 nM PLS peptide, in the presence of 0.5 μM $CuSO_4$ and 50 μM MG-132, a proteasome inhibitor (upper panel). Lower panel shows ETR1:HA in extracts using anti-HA antibody. (**d**) Densitometric scan of immunoblot. (**e**) Co-immunopreciptation of ETR1:HA (upper panel) in leaves of *N. benthamiana*, showing the effect of EDTA (to remove Cu) on interaction between ERT1:HA and PLS:GFP. Lower panels shows presence of ETR1:HA in extracts using anti-HA antibody, and protein input blots using anti-ETR1-HA and anti-Rubisco. (**f**) Densitometric scan of immunoblot. α-GFP, anti-GFP antibody; α-HA, anti-HA antibody. (**g**) Microscale thermophoresis binding curves of different ETR1 truncations with PLS. Binding of PLS was observed with full-length ETR1 and all C-terminal truncations but not with $ETR1^{306-738}$ lacking the N-terminal transmembrane part of the receptor.

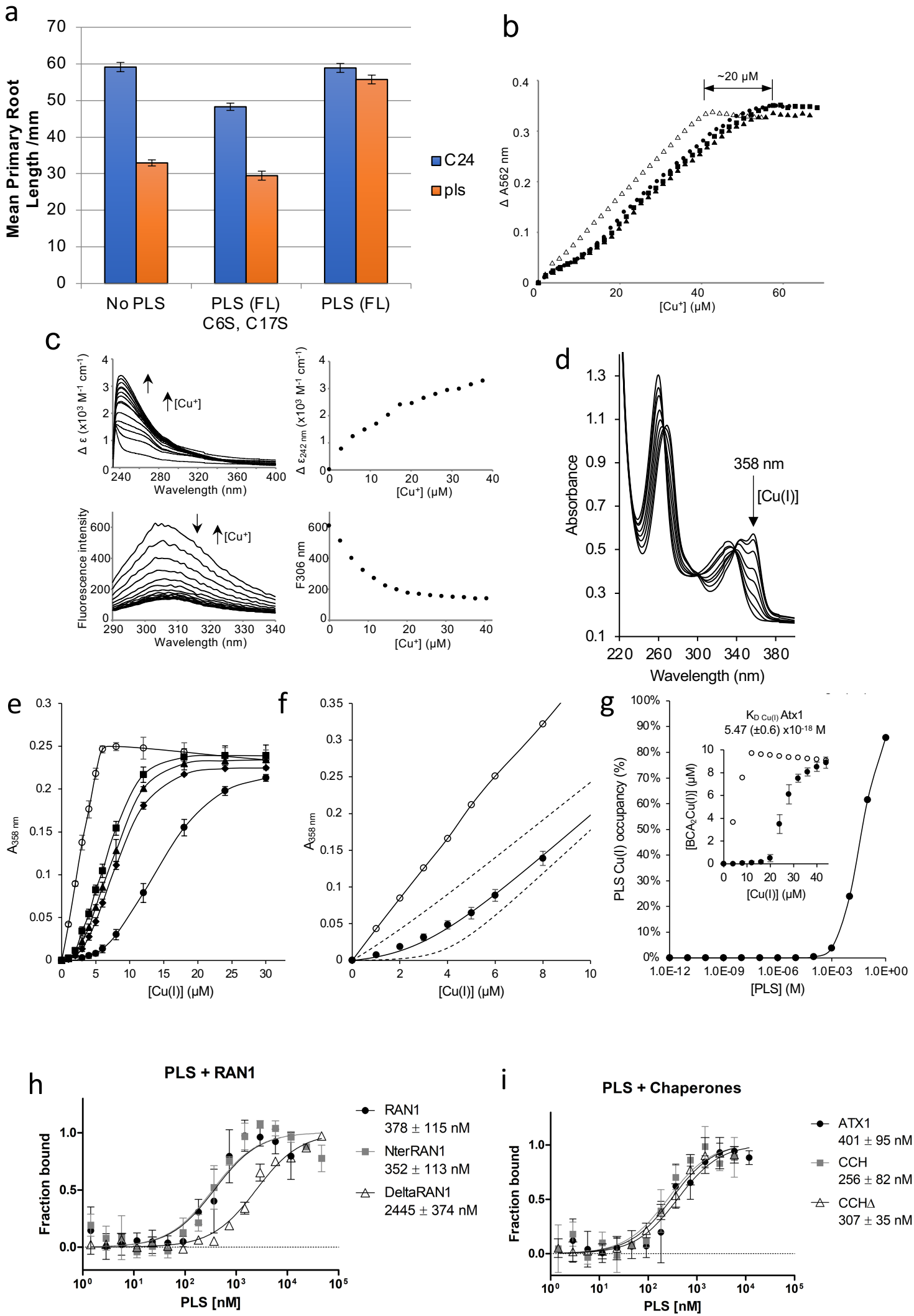
a
Mean Primary Root Length /mm
C24
pls
No PLS
PLS (FL)
PLS (FL) C6S, C17S
b
~20 µM
Δ A562 nm
[Cu+] (µM)
c
Δ ε (x10³ M⁻¹ cm⁻¹)
[Cu+]
Wavelength (nm)
Δ ε242 nm (x10³ M⁻¹ cm⁻¹)
Fluorescence intensity
F306 nm
d
Absorbance
358 nm
[Cu(I)]
Wavelength (nm)
e
A358 nm
[Cu(I)] (µM)
f
A358 nm
[Cu(I)] (µM)
g
KD Cu(I) Atx1
5.47 (±0.6) x10-18 M
PLS Cu(I) occupancy (%)
[BCA2Cu(I)] (µM)
[Cu(I)] (µM)
[PLS] (M)
h
PLS + RAN1
Fraction bound
RAN1
378 ± 115 nM
NterRAN1
352 ± 113 nM
DeltaRAN1
2445 ± 374 nM
PLS [nM]
i
PLS + Chaperones
Fraction bound
ATX1
401 ± 95 nM
CCH
256 ± 82 nM
CCHΔ
307 ± 35 nM
PLS [nM]

Figure 4. PLS binds copper and interacts with RAN1 and copper chaperones.
(**a**) C6S and C17S in PLS are required for function. Seedlings were grown hydroponically for 10 d in the presence (100 nM) or absence of peptide (FL or C6S, C17S). Blue bars are C24, red bars are *pls*. Asterisk: ANOVA, F2, 51 = 9.48, p = 3.15E-4, Tukey's HSD. Error bars show ± 1 standard error, n = 14-22. (**b**) BCA absorbance in the presence of synthetic PLS (19.8 μM, filled symbols) or an equivalent volume (to PLS) of DMSO (open symbols). Experiments with PLS used 88.3 μM (circles), 84 μM (triangles) and 88.4 μM (squares) BCA. The control experiment with DMSO used 85.3 μM BCA. (**c**) UV-vis apo subtracted difference spectra of synthetic PLS (19.8 μM) upon titration with CuCl (top left); binding isotherm of the feature at 242 nm (top right). Fluorescence spectra of PLS (19.8 μM) upon titration with CuCl (bottom left); binding isotherm of the feature at 306 nm (bottom right). (**d**) Absorption of BCA (17.3 μM) titrated with Cu(I) (representative spectrum, n = 2, full data in Fig S6). (**e**) Binding isotherms ($A_{358\ nm}$) of BCA (10 μM) in the presence/absence (filled/empty symbols, respectively) of 14 μM MBP-PLS (circles) or MBP-PLS mutants (C6S, C17S and C6S/C17S: triangles, diamonds and squares respectively) titrated with Cu(I) (n = 3, ±SD). (**f**) Binding isotherms ($A_{358\ nm}$) of BCA (50 μM) in the presence/absence of 10 μM MBP-PLS (filled/empty symbols, respectively) titrated with Cu(I). Model (solid line) describes Cu(I)-binding as a 2:1 complex, with β_2 affinity of 3.79 (±1.5) x10^{19} M^{-2}. Dotted lines simulate 10x weaker or tighter affinity (n = 3, ±SD). (**g**) Simulated Cu(I) occupancy (Supplementary Text) as a function of [PLS] using β_2 Cu(I) affinity of 3.79 x10^{19} M^{-2}. Inset, *Arabidopsis* ATX1 (20 μM, filled circles) withholds one Cu(I) equivalent from 20 μM BCA (open circles, BCA-alone) (n = 3, ±SD), with K_D Cu(I) 5.47 x10^{-18} M (Fig. S3). (**h**) Microscale thermophoresis binding curves of copper transporter RAN1 with PLS. (**i**) Microscale thermophoresis binding curves of soluble copper chaperones ATX1 and CCH with PLS (n = 3, ±SD).